JACS
JOURNAL OF THE AMERICAN CHEMICAL SOCIETY
Article
pubs.acs.org/JACS

EPR Spectroscopic Studies of the Fe−S Clusters in the O_2-Tolerant [NiFe]-Hydrogenase Hyd-1 from *Escherichia coli* and Characterization of the Unique [4Fe−3S] Cluster by HYSCORE

Maxie M. Roessler,[†,‡] Rhiannon M. Evans,[†] Rosalind A. Davies,[†] Jeffrey Harmer,*[,‡] and Fraser A. Armstrong*[,†,‡]

[†]Department of Chemistry and [‡]Center for Advanced Electron Spin Resonance, Oxford University, South Parks Road, OX1 3QR Oxford, United Kingdom

Supporting Information

ABSTRACT: The unusual [4Fe−3S] cluster proximal to the active site plays a crucial role in allowing a class of [NiFe]-hydrogenases to function in the presence of O_2 through its unique ability to undergo two rapid, consecutive one-electron transfers. This property helps to neutralize reactive oxygen species. Mechanistic details and the role of the medial and distal clusters remain unresolved. To probe the Fe−S relay, continuous wave and pulse electron paramagnetic resonance (EPR) studies were conducted on the O_2-tolerant hydrogenase from *Escherichia coli* (Hyd-1) and three variants with point mutations at the proximal and/or medial clusters. Reduction potentials of the proximal ($[4Fe-3S]^{5+/4+/3+}$) and medial ($[3Fe-4S]^{+/0}$) clusters were determined by potentiometry. The medial $[3Fe-4S]^{+/0}$ reduction potential is exceptionally high, implicating a mechanistic role in O_2-tolerance. Numerous experiments establish that the distal cluster has a ground state $S > 1/2$ in all three variants and indicate that this is also the case for native Hyd-1. Concurrent with the Hyd-1 crystal structure, EPR data for the 'superoxidized' P242C variant, in which the medial cluster is 'magnetically silenced', reveal two conformations of the proximal $[4Fe-3S]^{5+}$ cluster, and X-band HYSCORE spectroscopy shows two ^{14}N hyperfine couplings attributed to one conformer. The largest, $A(^{14}N) = [11.5,11.5,16.0] \pm 1.5$ MHz, characterizes the unusual bond between one Fe (Fe_4) and the backbone amide-N of cysteine-20. The second, $A(^{14}N) = [2.8,4.6,3.5] \pm 0.3$ MHz, is assigned to N_{C19}. The ^{14}N hyperfine couplings are conclusive evidence that Fe_4 is a valence-localized Fe^{3+} in the superoxidized state, whose formation permits an additional electron to be transferred rapidly back to the active site during O_2 attack.

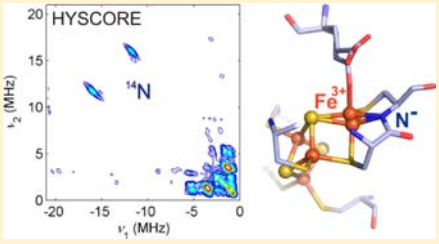

INTRODUCTION

Hydrogenases are metalloenzymes produced by microorganisms in which they catalyze the interconversion of H_2 and H^+.[1] The two major classes are known as [NiFe]- and [FeFe]-hydrogenases depending on the metals that are present at the active site,[1] and with turnover rates and catalytic efficiencies matching that of Pt,[2] they provide a paragon for H_2 production or oxidation by an extremely active catalyst based instead on first-row transition metals. The active sites are deeply buried in the protein, and an electron transfer (ET) relay is required to 'shuttle' electrons between the protein surface and the site of H_2 oxidation or reduction.[3] In a wider context, hydrogenases are members of a large group of enzymes that contain an extended relay of Fe−S clusters for intramolecular ET. A near-linear arrangement of the redox cofactors was first revealed in the [NiFe]-hydrogenase from *Desulfovibrio gigas*[4] and was subsequently discovered in many other enzymes, including fumarate reductase,[5] carbon monoxide dehydrogenase,[6] nitrate reductase[7] and NADH-quinone oxidoreductase (complex I).[8] Intramolecular ET along these relays can be very fast despite reaction coordinates often having large peaks and troughs as defined by the reduction potentials of each site.[9]

Recently, an intriguing and unprecedented role for the ET relay in certain hydrogenases has emerged: protection of the active site from damage initiated by O_2 attack.[10−19] Given the need for future renewable and sustainable energy technologies, it is no surprise that the mechanism enabling some hydrogenases to sustain catalysis in air is now the subject of intense research.[11,13,14,18,19]

Three recent crystal structures of such O_2-tolerant respiratory [NiFe]-hydrogenases reveal a highly unusual Fe−S cluster proximal to the active site (Figure 1),[10,16,17] which owing to its special ability to cycle between *three* oxidation states,[14] is capable of a dual role. During H_2-oxidation catalysis, this $[4Fe-3S]^{5+/4+/3+}$ cluster together with the medial $[3Fe-4S]^{+/0}$ and distal $[4Fe-4S]^{2+/+}$ clusters mediates efficient ET from the active site to the protein surface. Crucially, when O_2 attacks, the proximal cluster can access the '5+' level and rapidly discharge two 'rescue' electrons *back* to the active site, thus helping to ensure complete reduction of the O_2 molecule. This mechanism neutralizes reactive oxygen species that would otherwise be trapped in the active site.[11,13,14] As a consequence

Received: July 20, 2012
Published: August 19, 2012

   dx.doi.org/10.1021/ja307117y | *J. Am. Chem. Soc.* 2012, 134, 15581−15594

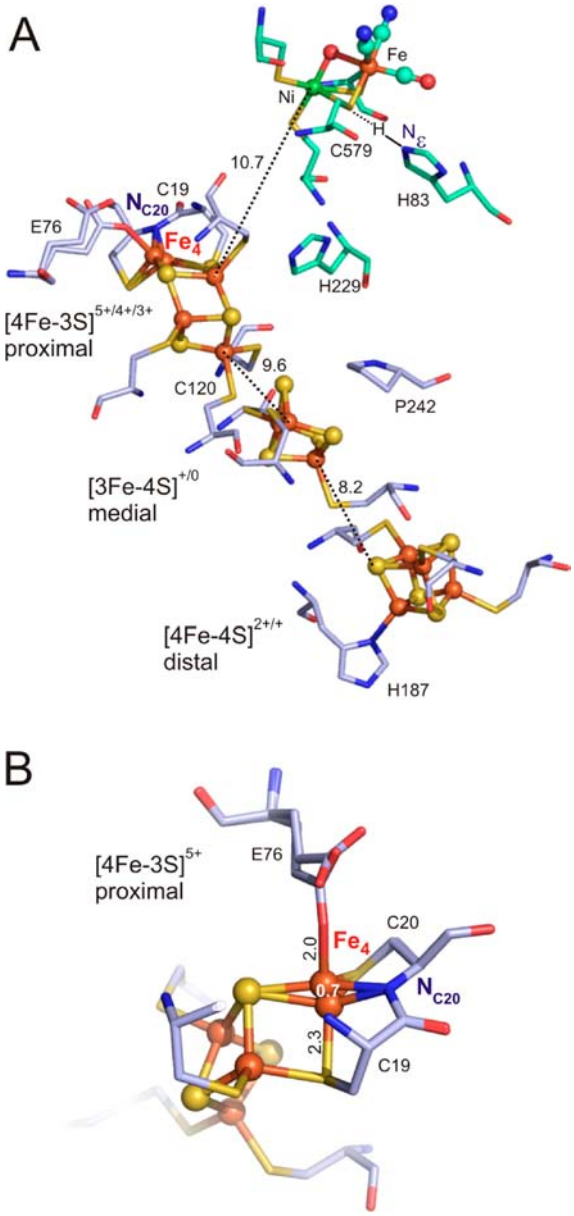

Figure 1. Amino acid environment of the Fe–S clusters (small subunit, blue) and active site (large subunit, green) (PDB 3USC) in *Ec* Hyd-1 at high potential (A) and detailed view of the proximal [4Fe–3S]$^{5+}$ cluster illustrating its conformational change (B). Fe_4 and Glu76 can adopt at least two conformations (see ref 17). (A) The position of the H atom in the hydrogen bond between Cys579 and Nε of His83 is approximate. Edge-to-edge intercluster distances are given in Å. (B) Close-up of the proximal cluster from a different viewpoint, illustrating the oscillation of Fe_4 (by 0.7 Å) between E76 and C19. Bond distances of the Fe_4 closest to E76 or C19 are given in Å.

of this process, O_2-tolerant respiratory hydrogenases form only the resting state called Ni–B, also known as 'Ready' (a Ni^{3+}–OH species)[20] when exposed to O_2 during H_2 oxidation: Ni–B reactivates rapidly upon one-electron reduction enabling normal catalysis to be resumed.[21] Otherwise, incomplete reduction of O_2 results in states known as 'Unready' that reactivate only slowly, and H_2 oxidation is not possible under aerobic conditions. One of these 'Unready' states, characterized spectroscopically and known as Ni–A (also a Ni^{3+} species) is usually only associated with O_2-sensitive hydrogenases, although 'as-isolated' O_2-tolerant hydrogenase-1 from *Escherichia coli* (*Ec* Hyd-1) that has not been grown and purified under H_2 is typically found in a mixture of Ni–A and Ni–B[12] and other 'Unready' states.[13]

Amino acid sequences of O_2-tolerant membrane-bound hydrogenases show two 'supernumerary' cysteines in the region of the unusual proximal cluster (numbered C19 and C120 in *Ec* Hyd-1 and the hydrogenase from *Ralstonia eutropha*, *Re*-MBH) which correspond to conserved glycines in standard (O_2-sensitive) hydrogenases.[11,13−15] These cysteines play a crucial role in conferring O_2-tolerance.[11,13] Recent crystal structures[10,16,17] reveal their direct ligation to the proximal [4Fe–3S] cluster where C19 provides the fourth sulfur ligand in place of the normally encountered S^{2-} (Figure 1). Electrochemical experiments have demonstrated that the substitution of C19 for a glycine makes the enzyme very O_2-sensitive, even to very low levels of O_2,[13] and the ability of the C19G/C120G variant of *Re*-MBH or *Ec* Hyd-1 to function in O_2 was also greatly compromised.[11,13]

The crystal structures of native *Hydrogenovibrio marinus* (*Hm*) MBH[16] and *Ec* Hyd-1[17] reveal that the upper redox transition of the proximal cluster ([4Fe–3S]$^{5+/4+}$) involves an intriguing atomic rearrangement. In the superoxidized [4Fe–3S]$^{5+}$ form, one of the Fe atoms (Fe_4 in Hyd-1, Figure 1B) becomes coordinated by a peptide backbone amide nitrogen from cysteine-20 (N_{C20}) in both cluster conformations that are revealed.[17] The nature of the N_{C20}–Fe_4 bond and electronic state of Fe_4 in the superoxidized form are of great interest. As we will describe in this paper, HYSCORE (hyperfine sublevel correlation) spectroscopy experiments on a medial cluster variant of Hyd-1 (P242C) reveal that Fe_4 is valence localized in the +3 oxidation state, as recently proposed based on quantum mechanics/molecular mechanics calculations.[17] The P242C mutation, designed to convert the medial [3Fe–4S] cluster into a [4Fe–4S] cluster, decreases the number of interacting paramagnets and simplifies the complex spectrum of O_2-tolerant hydrogenases that is obtained at high potential.[11,13−15,22]

Although the proximal cluster seems to play the most important role in determining the O_2-tolerance of membrane-bound [NiFe]-hydrogenases, it is noteworthy that the reduction potentials of all three Fe–S clusters are reported to be shifted to higher values in O_2-tolerant hydrogenases[14,23,24] compared to their O_2-sensitive counterparts from the *Desulfovibrio* family.[19] Unlike the proximal cluster, the structures of the medial [3Fe–4S] and distal [4Fe–4S] clusters in the O_2-tolerant enzymes are similar to those found in O_2-sensitive hydrogenases.[10,16,17]

The role of the reduction potential of the medial cluster has been investigated in the O_2-sensitive hydrogenase from *Desulfovibrio fructosovorans*.[25] A [3Fe–4S]$^{+/0}$ cluster usually has a much more positive reduction potential than a [4Fe–4S]$^{2+/+}$ cluster and will tend to trap an electron at the medial site.[25−30] In all membrane-bound [NiFe]-hydrogenases studied to date, a proline (P238 in *Df* hydrogenase, P242 in *Ec* Hyd-1, Figure 1) occupies the position a cysteine would occupy in [NiFeSe]-hydrogenases (Figure S1), which instead contain a [4Fe–4S] cluster in the medial position. Rousset et al.[25] found that the catalytic activity of the *Df* P238C variant, containing a medial [4Fe–4S] cluster, was only slightly decreased compared to that of the native enzyme, despite a drop of ~300 mV in the reduction potential of the medial cluster.

The possible importance of all Fe–S clusters in conveying O_2-tolerance prompted us to investigate the ET relay in O_2-

tolerant *Ec* Hyd-1[12] as an entire entity, making use of several variants to probe different parts of the Fe−S cluster chain using electron paramagnetic resonance (EPR)-based potentiometric titrations. In addition to the proximal C19G/C120G and the medial P242C variants, we constructed and characterized the triple C19G/C120G/P242C variant, which combines amino acid substitutions at both the proximal and medial Fe−S clusters. We also employed a powerful Eu(II) reducing agent to probe for the presence of Fe−S clusters with very low reduction potentials.[31−35]

The distal $[4Fe{-}4S]^{2+/+}$ cluster, which is ligated by one histidine and three cysteine residues (Figure 1A), should set the potential at which the rest of the ET relay operates since it is the entry point for electrons into the enzyme from the natural redox partner, cytochrome.[15,25,36,37] Knowledge of its reduction potential is therefore paramount. Following recent electrochemical studies,[38] the distal cluster in Hyd-1 is expected to have a relatively high reduction potential and ought to be easily detectable by EPR provided the reduced cluster has a $S = 1/2$ spin ground state. However, proximal cluster variants of both *Re*-MBH and *Ec* Hyd-1 lack any Fe−S cluster continuous wave (CW) EPR signals around $g = 2$ at low potentials, suggesting that the distal $[4Fe{-}4S]^{+}$ cluster does not have a $S = 1/2$ ground state.[11,13] This is an important issue that we investigate in detail.

This paper presents a consolidated picture of the ET relay of an O_2-tolerant hydrogenase, based upon the EPR spectra of the Fe−S clusters in the different Hyd-1 variants and unravelling the complex couplings that occur whenever paramagnets are in close proximity. In particular, the results provide insight into the properties of the intriguing proximal $[4Fe{-}3S]$ cluster.

METHODS

Preparation of EPR Samples. All EPR samples were prepared in 0.10 mM 2-(*N*-morpholino)ethanesulfonic acid (MES), 0.10 mM NaCl, 10% (v/v) glycerol, adjusted to pH 6.0 at 20 °C (henceforth 'MES buffer'). All samples for the spectra shown in Figure 2 and Figures S2−4 result from 'as-isolated' enzyme titrated to the desired potential under Ar with substoichiometric quantities of potassium ferricyanide and sodium dithionite, as described previously.[13] The following mediators, at a final concentration of 40 μM each, were employed: methyl viologen, benzyl viologen, phenazine methosulfate, indigotetrasulfonate, 1,2-naphthoquinone, and 2-hydroxyl-1,4-naphthoquinone. All samples were prepared in high-precision EPR tubes (Wilmad 714-PQ-7) to ensure accurate spin quantification (see below). Total protein concentration was estimated spectroscopically using the method of Bradford,[39] with bovine serum albumin (Sigma-Aldrich, stock concentration 2 mg BSA/mL) as the protein standard.

The low-potential native Hyd-1 sample (Figures 3 and 4) was prepared in an anaerobic glovebox (O_2 < 1 ppm, Glove Box Technology) by H_2-reducing approximately 200 μL as-isolated enzyme in 100% H_2 at 37 °C for 2 h before returning the temperature to 20 °C. An aliquot (1−2 μL) of the solution was transferred as quickly as possible to a W-band EPR tube (Wilmad S-.7X.87), approximately 80 μL was transferred to a 3.8 mm tube (Wilmad 706-PQ) for X-band field sweep and HYSCORE measurements, and finally an aliquot of approximately 50 μL was transferred to a 3 mm tube (CE-MAT PN99553627) suitable for double electron−electron resonance (DEER) measurements. A portion of the Hyd-1 enzyme sample was retained to determine the concentration (555 μM). The low-potential P242C and C19G/C120G samples (Figures 3 and 4) were prepared in a similar way, except that 150 μL (the minimum solution volume required to read an accurate potential) of as-isolated enzyme containing 200 μM each of the six mediators detailed above, was adjusted to −250 and to −200 mV, respectively, by addition of sodium dithionite. Only an approximate concentration is given (0.30 mM) because several samples of known concentration were pooled and reduced to the desired volume. A sample of H_2-reduced P242C (Figure 5) was prepared by saturating as-isolated enzyme under 100% H_2 for 2 h at 37 °C; the temperature was then returned to 20 °C before freezing in an EPR tube. Note that the purpose of saturating both Hyd-1 and P242C with H_2 was *not* to fully activate the enzyme (i.e., remove Ni−A and other Unready states), which would require much longer times.[13]

Highly reduced samples of P242C and C19G/C120G/P242C (Figure 5, see also Figure S9) were prepared by adding tiny aliquots (0.2−0.4 μL) of equimolar quantities of $EuCl_2$ (Sigma Aldrich, stored in an anaerobic atmosphere) and diethylene triamine pentaacetic acid (DTPA, Alfa) simultaneously to the H_2-saturated enzyme solution (see SI for details). Due to the air sensitivity of Eu(II), all experiments were conducted in an anaerobic glovebox (O_2 < 1 ppm, Glove Box Technology). Stable potentials could only be obtained under a H_2 atmosphere, which ensures that the enzyme is product inhibited and unable to turn over.[12] To measure the solution potential, a pyrolytic graphite edge electrode was used with a Ag/AgCl electrode as reference (Figure S8). All potential values are given with reference to the standard hydrogen electrode using the conversion $E_{SHE} = E_{Ag/AgCl}$ + 204 mV at 20 °C.

The sample of P242C (622 μM) oxidized to +381 mV for pulse X-band measurements (Figures 7 and 8) contained 400 μM each of phenazine methosulfate, 1,2-naphthoquinone, and indigotetrasulfonate. The potential was adjusted by addition of substoichiometric quantities of 400 mM $K_3[Fe(CN)_6]$ in an anaerobic titration cell on the bench.[13] The sample was then transferred to an EPR tube (Wilmad 706-PQ), which was previously equilibrated with the gas atmosphere of the titration cell, and flash frozen in an isopropanol slush.[13] The W-band sample of P242C in Figure 8 was prepared in a titration cell in an anaerobic glovebox (O_2 < 1 ppm, Glove Box Technology) by adjusting ca. 100 μL as-isolated enzyme (250 μM) containing 50 μM each of phenazine methosulfate, 1,2-naphthoquinone, and indigotetrasulfonate to a potential of +373 mV. An aliquot of solution (1−2 μL) was transferred as quickly as possible to a W-band EPR tube (Wilmad S-.7X.87) and flash frozen. Although the potential was steady as the enzyme solution was transferred to the EPR tube, the potential of W-band samples was generally found to be less reliable than that of X-band EPR samples and should therefore be considered as approximate.

Potentiometric EPR Titrations ('Nernst plots'). The height of a signal at a particular field position (g value) in a CW EPR spectrum was determined by averaging the values within a small field range either side of the g value of interest (see dotted vertical lines in Figures S2−S4). The maximum peak intensity was set to 1 for all species monitored (except the medial $[3Fe{-}4S]^{+}$ cluster peaks in native Hyd-1) following the results of the spin quantifications (see Figure 2). Field positions belonging to the same species, which give rise to similar peak-intensity vs potential ('Nernst') plots, are indicated by vertical dotted lines of the same color in Figures S2−S4. Only one of the lines of the same color is shown in Figure 2. Solid lines based on the one-electron Nernst equation were fitted to the experimental data points by inspection (with exception of the medial cluster in native Hyd-1). The error of the fit was also judged 'by eye' from peak intensities at several different field positions of the same species. In native Hyd-1, the potential at which uncoupled $[3Fe{-}4S]^{+}$ cluster signals are observed at their maximal intensity does not correspond to the medial cluster being 100% oxidized. The 'true' midpoint potential of the medial cluster in native Hyd-1 was determined from spin integrations as detailed in Figure S7.

Spin Quantification. Spin quantification was carried out as previously described[13] using a calibration graph obtained with copper perchlorate samples (20, 50, 100, 150, and 200 μM $CuSO_4$ in 2 M $NaClO_4$(aq) adjusted to pH 1.22 with HCl) measured under nonsaturating conditions.

EPR Spectroscopy. CW EPR experiments were performed using an X-band (9.1−9.9 GHz) Bruker EMX spectrometer (Bruker BioSpin GmbH, Germany) with an X-band superhigh-sensitivity probehead (Bruker). The field was calibrated at room temperature with 2,2-

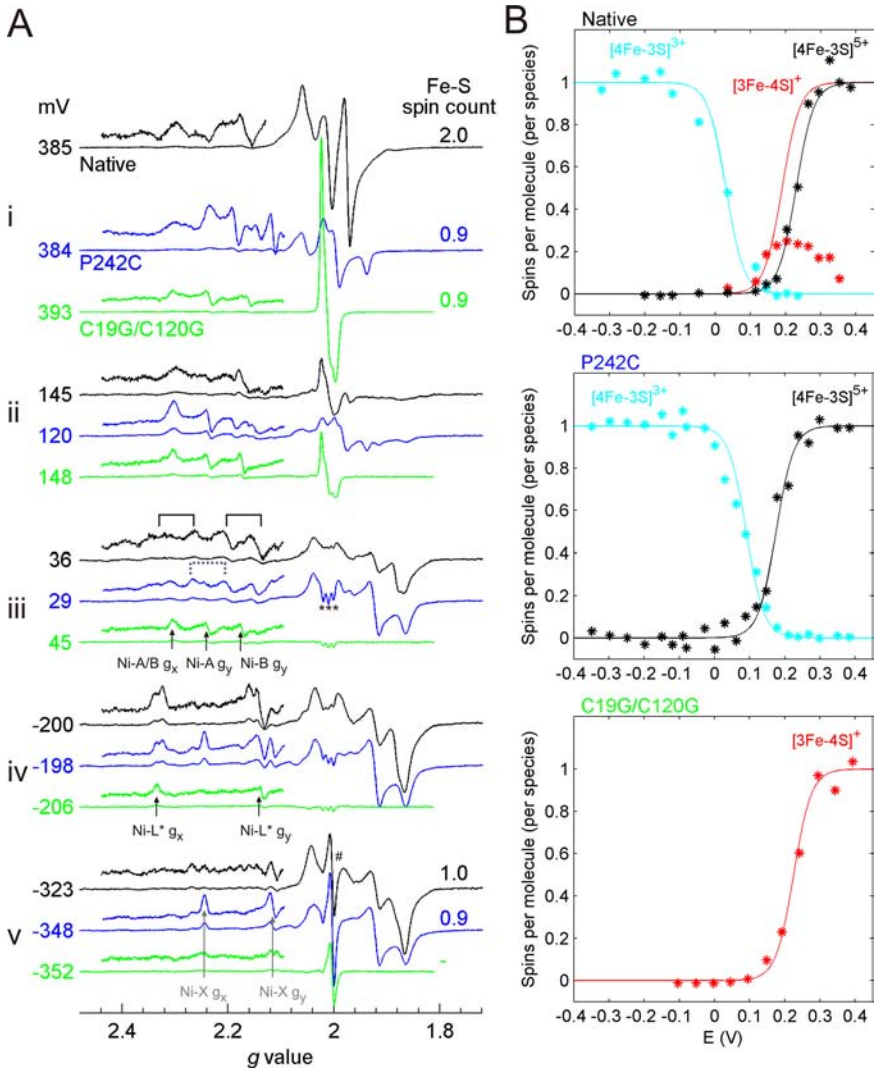

Figure 2. X-band CW EPR spectra of native Hyd-1 (15 K), P242C (20 K) and C19G/C120G (15 K) poised at selected potentials and potentiometric titrations of the EPR-active species. (A) Annotations refer to the potential at which the samples were taken (left, in mV) and spin integrations of the Fe−S cluster region (right). For measurement conditions see Figures S2−4, which show the complete set of EPR spectra at the potentials used for the plots in (B). Spectra of P242C were measured at 20 K, as signals (which did not change shape between 3.4 and 30 K; Figure S5) became saturated more easily than with the native enzyme. (B) Peak intensities of the EPR active species as a function of potential, fitted to the one-electron Nernst equation with midpoint potentials given in Table 1. Peak positions in the CW EPR spectra used to give the peak intensities are detailed in Figures S2−4. A more conventional way of depicting the [3Fe−4S] cluster transitions in native Hyd-1 is given in Figure S6A. For the P242C $[4Fe-3S]^{5+}$ 'Nernst plot', monitoring peak intensities at different field positions resulted in a spread of reduction potentials of ca. 55 mV (Figure S6B). Unidentified peaks are marked with an asterisk.[13] These may be due to a nitroxide radical or trace amounts of free Fe^{3+} coordinated to a ^{14}N nucleus and have been observed previously in preparations from other O_2-tolerant hydrogenases.[47,78] Peaks arising from methyl and benzyl viologen are marked with #. Unsplit g_x and g_y of Ni−A, Ni−B and Ni−L* are indicated; those of Ni−X are shown in gray, as the origin of this species is not understood and was not investigated further here.

diphenyl-1-picrylhydrazyl as an external standard (g = 2.0036). Background spectra of the empty resonator were recorded under identical conditions and subtracted from the EPR spectrum of the enzyme sample. Most pulse measurements were carried out on a W-/X-band Bruker Elexsys 680 spectrometer using an X-band EN-4118 MD4 resonator or a W-band EN 600−1021H TeraFlex resonator. Some X-band pulse measurements were carried out on a X-band Bruker 580 spectrometer at the National EPR Research Facility and Service in Manchester, with a MD4-W1007 resonator. All spectrometers were equipped with low-temperature helium flow cryostats (Oxford Instruments). The W-band B_0 field was calibrated via a Mims electron-nuclear double-resonance (ENDOR) measurement of the proton nuclear Zeeman frequency. The Cu^{2+} and Mn^{2+} signals from the empty W-band resonator are significant, as seen in Figures 3 (bottom) and 8B. In particular, the Mn^{2+} signals can mask important Fe−S cluster signals around the g = 2 region, and a simple subtraction of the background spectrum from the enzyme sample spectrum is difficult. This background signal could not be removed or even significantly suppressed experimentally (with, e.g., flip angle techniques),[40] since it is present in the W-band cavity body and hence at a different position to the enzyme sample.

Hydrogenase Preparation: Expression of HyaA and Purification of Gene Products. Native and variant Hyd-1 enzymes were purified from MC4100[41]-derived *E. coli* K-12 strain FTH004.[42] This strain carries an engineered hyaABCDEF operon encoding a modified HyaA protein bearing a His_6 affinity tag at its extreme C terminus (Table S1). Details of the *E. coli* strains and the production of the variant enzymes are supplied in SI and as previously published.[13] Purification of all enzymes was achieved essentially as described earlier,[12,13] by application of solubilized membrane pellets to a Ni^{2+}-

dx.doi.org/10.1021/ja307117y | J. Am. Chem. Soc. 2012, 134, 15581−15594

Table 1. Midpoint Potentials of the EPR-Active Fe−S Clusters Observed in Native Hyd-1, the P242C, and C19G/C120G Variants Compared to Other Native O_2-Tolerant Hydrogenases[a]

enzyme	$[4Fe-3S]^{5+/4+}$ proximal	$[4Fe-3S]^{4+/3+}$ proximal	$[3Fe-4S]^{+/0}$ medial	$[3Fe-4S]^{+/0}_{app.}$ medial	$[4Fe-4S]^{2+/+}$ distal
native Hyd-1	230 ± 15	30 ± 30	190 ± 30	130 ± 15	–
P242C	175 ± 15[b]	90 ± 20	–	–	–
C19G/C120G	–	–	215 ± 10	–	–
Aa Hase I[14]	232 ± 20	98 ± 20	–	78 ± 20	−65 ± 20
Re-MBH[23]	160	–	–	25	−60
Rm CH34[23]	240	–	–	100	50

[a]The midpoint potentials are given in mV vs SHE, were obtained as detailed in Methods section, and reflect the 'Nernst plots' given in Figure 2B. The potentials for *Aa* Hase I were obtained at pH 6.4 vs the normal hydrogen electrode,[14] and those for *Re*-MBH and *R. metallidurans* CH34 were obtained at pH 7.0.[23] All potentials for the Hyd-1 enzymes were obtained at pH 6.0. The apparent midpoint potential ('app') refers to the potential at which the uncoupled $[3Fe-4S]^{+}$ cluster signal is at half its maximum intensity (Figure S6A). [b]Monitoring peak intensities at different field positions resulted in a spread of reduction potentials of ca. 55 mV (Figure S6B).

loaded 5 ml HisTrap chelating HP column (Amersham Biosciences), substituting detergents *n*-dodecyl-*β*-D-maltoside (0.02% w/v) for Triton X-100 (0.02% w/v) throughout.

RESULTS

Titrations. Figure 2A summarizes the CW EPR spectra of native Hyd-1 (black), P242C (blue), and C19G/C120G (green) at selected potentials (see Figures S2−S4 for full titrations). The Fe−S cluster signal intensities were monitored as a function of potential and fitted to the one-electron Nernst equation with appropriate midpoint potentials to yield the three 'Nernst plots' shown in Figure 2B. Detailed inspection of the data obtained with P242C (Figure S3) showed differences in the Nernst plots of the high-potential redox transition depending on the *g* value chosen, and the data in Figure 2B (middle, black curve) result from peak intensities at $g = 2.062$. As shown in Figure S6, a spread of ca. 55 mV was found, and this significant result is discussed later.

The spectrum at 15 K of highly oxidized native Hyd-1 (Figure 2Ai, black line, see also ref 13) displays complicated magnetic interactions between the active site (Ni−A or Ni−B, $S = 1/2$), the proximal $[4Fe-3S]^{5+}$ cluster ($S = 1/2$) and the medial $[3Fe-4S]^{+}$ cluster ($S = 1/2$), as typically observed for O_2-tolerant [NiFe]-hydrogenases.[11,13−15] In the P242C variant (blue line) a $[4Fe-4S]^{2+}$ cluster ($S = 0$) should be present in place of the $[3Fe-4S]^{+}$ cluster; consequently no signal or magnetic interactions are expected from the medial cluster. Indeed, the Fe−S cluster region in the 20 K spectrum now integrates to 0.9 ± 0.3 spins per molecule, compared to 2.0 ± 0.3 in the native enzyme. As previously shown,[11,13] replacement of both 'supernumerary' cysteine residues by glycines at the proximal cluster (C19 and C120 in Hyd-1) causes the proximal cluster to lose its ability to undergo the high-potential $[4Fe-3S]^{4+}$−$[4Fe-3S]^{5+}$ transition. Thus only the uncoupled $[3Fe-4S]^{+}$ medial cluster signal is observed in high-potential samples of the C19G/C120G variant (green line), and this integrates to 0.9 ± 0.2 spins per molecule. Most definitively, the C19G/C120G/P242C variant, which combines amino acid substitutions at both the proximal and medial clusters, shows no Fe−S cluster EPR signals at high potentials, fully consistent with a [4Fe−4S] cluster occupying the medial position (Figure S10). Like the other variants of Hyd-1,[13] P242C and C19G/C120G/P242C are intensely colored and catalytically active (Table S4). For native Hyd-1 and the P242C variant, only *one* low-potential Fe−S cluster redox transition is observed and is assigned to the proximal cluster $[4Fe-3S]^{4+/3+}$ couple (vide infra). The potential dependent changes in the EPR spectra are now discussed in detail.

Because the proximal Fe−S cluster should be structurally and electronically the same (and environmentally similar) in native Hyd-1 and P242C, the high-potential redox transition (Figure 2B, black) with a midpoint potential of +230 ± 15 mV in native Hyd-1 and +175 ± 15 mV in P242C is assigned to the proximal cluster $[4Fe-3S]^{5+/4+}$ couple (Table 1). The spectra of C19G/C120G (Figure 2Ai, green line) and C19G/C120G/P242C (Figure S10) at 15 K are consistent with this interpretation as they exhibit uncoupled Ni−A and Ni−B signals. The spectra contrast with those recorded for the native and P242C enzymes, in which the Ni signals at low temperature are split by a very large exchange interaction ($J \sim 600$ MHz) with the proximal $[4Fe-3S]^{5+}$ cluster (Figure 2Ai, see also Figure 8). At high temperature (70 or 80 K) where Fe−S cluster signals are not observed, the Ni−A and Ni−B signals are not split (Figure S11). However, the Ni−A/Ni−B intensity is much lower in native Hyd-1 and P242C compared to C19G/C120G and C19G/C120G/P242C (not shown), an observation that is attributed to spin relaxation as a result of the nearby paramagnetic $[4Fe-3S]^{5+}$ cluster.

The data points tracing a bell-shaped curve in Figure 2B (top, red stars) correspond to the uncoupled $[3Fe-4S]^{+}$ medial cluster signals in native Hyd-1 ($g_{x,y,z} = 2.03, 2.01, 2.00$). The decrease in amplitude at high-potential should not be interpreted as the $[3Fe-4S]^{+}$ medial cluster signals becoming EPR silent but reflects a strong exchange coupling between the proximal and medial clusters that manifests itself as a complex interaction EPR spectrum. In native Hyd-1 the $[3Fe-4S]^{+}$ cluster is only observed uncoupled from the proximal cluster up to a moderately high potential (+145 mV, Figure 2Aii, black line). At this potential the signals due to Ni−A and Ni−B are not split because magnetic interactions between the medial $[3Fe-4S]^{+}$ cluster and the active site Ni(III) species are negligible.[11,13] In the C19G/C120G variant (green line), the medial cluster signals are not affected by magnetic interactions since the proximal cluster is EPR silent, and the true midpoint potential can therefore be determined, Figure 2B (bottom). No peaks attributable to a $[3Fe-4S]^{+}$ cluster are visible at any potential in the titration of P242C (blue lines, see also Figure S3).

The spectra in Figure 2Aiii result from samples poised at a potential where the medial $[3Fe-4S]^{+}$ cluster (in native Hyd-1 and C19G/C120G) is reduced and the low-potential proximal [4Fe−3S] or distal [4Fe−4S] cluster is partially reduced, while the inactive EPR-visible Ni species are still partially oxidized

dx.doi.org/10.1021/ja307117y | J. Am. Chem. Soc. 2012, 134, 15581−15594

(Ni−A and Ni−B). Whereas the Fe−S cluster signals in native Hyd-1 (black line) display at least four features (turning points) and are complicated, a simple rhombic EPR signal appears in P242C (blue line), and no signals are visible in C19G/C120G (green line). In the absence of magnetic coupling from Fe−S clusters in the C19G/C120G variant spectrum, Ni−A and Ni−B are easily identifiable. This is not the case for native Hyd-1 or P242C. Since as-isolated native Hyd-1 contains little Ni−A (Figure S11), the observed Ni signals in Figure 2Aiii must result principally from Ni−B. Both Ni−B g_x and g_y features are split symmetrically and to a similar extent into doublets of approximately equal intensity (as indicated in Figure 2Aiii), as a result of an isotropic exchange interaction of ca. 110 MHz between the active site and a nearby Fe−S cluster. For P242C, the Ni region of the spectrum is very similar to that of the native enzyme, and the exchange interaction between Ni−B and the reduced Fe−S cluster is ca. 100 MHz. However, the P242C variant also contains a substantial amount of Ni−A (Figure S11), and the exchange interaction between Ni−A and the reduced cluster in P242C is likely to be of similar magnitude; the unsplit Ni positions are evident from the C19G/C120G variant (green line). At 80 K, in the absence of detectable Fe−S cluster signals due to fast relaxation, unsplit Ni−A and Ni−B signals are observed for native Hyd 1 and P242C (Figure S11). This observation shows that the coupling originates from an interaction with the reduced proximal cluster and not the distal cluster which is too distant from the active site (Figure 1) to produce a splitting of this magnitude.

Upon further reduction (Figure 2Aiv), the reduced Fe−S cluster signals observed in native Hyd-1 and the P242C variant intensify. The signal shape in the native enzyme changes with potential, and this is discussed further below. A Ni species with $g_{x,y,z}$ = 2.33, 2.14, 2.05 (named Ni−L*, see Discussion section and Figure S12) and with maximum signal intensity at approximately −200 mV (at pH 6) is observed in all Hyd-1 enzymes. A splitting in the g_x component of ∼49 MHz in native Hyd-1 and 42 MHz in P242C, which disappears at high temperatures (Figure S11), indicates that Ni−L* is magnetically coupled to another species. There are two peaks observed around g_y, but this is not the result of an interaction with a Fe−S cluster since it is also present at high temperature. The size and anisotropy of the splitting at low temperature indicate a significant electron−electron dipolar interaction which can only arise from the nearby proximal cluster (Figure 1A). Further evidence for this interpretation is provided by the unsplit Ni−L* spectrum observed in variants C19G/C120G (Figure 2Aiv), C19G and C120G (Figure S13), for which the proximal cluster is EPR silent.[13] The W-band signal positions of Ni−L* (Figure 3, top, g_x = 2.33) confirm that the splitting of the g_x peak at X-band is due to a dipolar interaction with the reduced proximal cluster.

At potentials comparable to those reached by H_2 reduction (Figure 2Av), signals arising from Ni−L* have disappeared (due to further reduction of the active site to an EPR-silent state known as Ni−R), but P242C (blue line) exhibits signals at $g_{x,y,z}$ = 2.24(5), 2.11(5), 2.05 (marked in gray as Ni−X in Figure 2Av) which are present at a much smaller intensity in native Hyd-1 (black line) and C19G/C120G (green line). The Fe−S cluster region of native Hyd-1 and P242C integrates to 1.0 ± 0.2 and 0.9 ± 0.2 spins per molecule of enzyme, respectively. This fact eliminates the possibility that the low-potential redox transition (Figure 2B, top/middle) observed in the titration of these enzymes results from several clusters with exactly the same midpoint potential. The EPR spectrum of C19G/C120G at −352 mV (green line) does not exhibit *any* Fe−S cluster EPR signals in the g = 2 region, suggesting that the distal cluster (as well as the proximal cluster) is EPR silent. It is highly unlikely that point mutations in the proximal cluster would result in a change of the spin state of the distal cluster, which is more than 20 Å away (Figure 1A). Consequently, the absence of S = 1/2 EPR signals in C19G/C120G provides compelling evidence that the Fe−S cluster redox transition observed at low potential for native Hyd-1 and P242C is due to the proximal $[4Fe{-}3S]^{4+/3+}$ couple. The titration data make it extremely unlikely that the distal $[4Fe{-}4S]^{+}$ cluster has a S = 1/2 ground state in any of the Hyd-1 enzymes. In addition, the $[4Fe{-}4S]^{+}$ medial cluster in Hyd-1 P242C also appears to be EPR silent. Additional experiments to investigate the ET relay at low potentials are presented below.

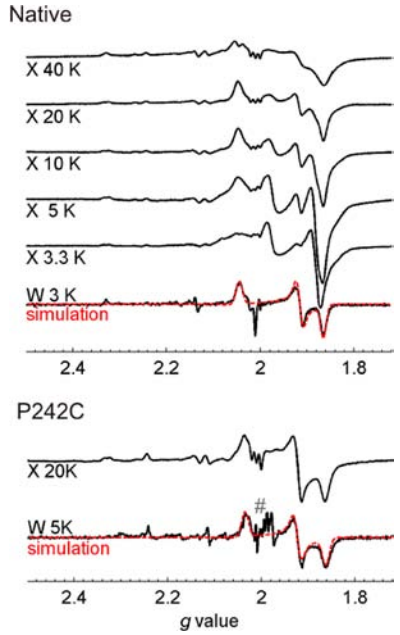

Figure 3. Comparison of low-potential native Hyd-1 and P242C at X- and W-band. (Top) X-band CW EPR spectra showing the temperature dependence of low-potential species in native Hyd-1 and the numerical derivative of the echo-detected W-band spectrum. All X-band spectra amount to approximately one spin per molecule of enzyme (Table S5). (Bottom) X-band CW EPR and numerical derivative of echo-detected W-band spectra of P242C. Measurement conditions: (X-band, native) mw power 2 mW (40 K), 0.5 mW (20 K), 0.12 mW (10 K), 32 μW (5 K), 8 μW (3.3 K), modulation amplitude 1 mT (all), 9.381 GHz; (X-band, P242C): mw power 0.5 mW, modulation amplitude 1 mT, 9.375 GHz; (W-band, native): pulse sequence $\pi/2 - \tau - \pi - \tau -$ echo where τ = 180 ns and $\pi/2$ = 32 ns, 93.839 GHz, shot repetition time 5 ms, 2-step phase cycle; (W-band, P242C): pulse sequence $\pi/2{-}\tau{-}\pi{-}\tau{-}$echo, where τ = 180 ns and $\pi/2$ = 28 ns, 93.859 GHz, shot repetition time 5 ms, 2-step phase cycle. Sample concentrations: 555 μM (native), approximately 300 μM (P242C, W-band), 46 μM (P242C, X-band). Peaks arising from Mn^{2+} present in the spectrometer cavity are marked with #. W-band Fe−S EPR spectra were simulated (red dotted lines) with $g_{x,y,z}$ = 2.045, 1.916, 1.865 (native) and $g_{x,y,z}$ = 2.035, 1.923, 1.862 (P242C).

Assignment of the Low-Potential Fe−S EPR Spectra. At low potential it is clear from the data in Figure 2 that the proximal cluster has a S = 1/2 ground state in both native Hyd-1 and the P242C variant. Identification of the distal Fe−S spectrum has proven elusive in our work. The evidence below

dx.doi.org/10.1021/ja307117y | J. Am. Chem. Soc. 2012, 134, 15581−15594

unambiguously establishes that the reduced distal cluster in the variants of Hyd-1 (P242C, C19G/C120G and C19G/C120G/P242C) has a ground state $S \neq 1/2$. The data for native Hyd-1 also point very strongly to this conclusion, but we stop short of stating this as a fact without a satisfactory simulation of the temperature dependence of the X-band CW EPR signals (Figure 3, see below). The evidence for this conclusion is now summarized:

(1) The shape of the Fe−S cluster signals in low-potential Hyd-1 samples (Figure 2Aiii−v) is complex and changes significantly as a function of temperature, as shown in Figure 3 (top). In contrast, the shape of the Fe−S region of the EPR spectrum of reduced P242C does not change with decreasing temperature (Figure S14). Notably, double integration of the Fe−S cluster EPR signals of both native Hyd-1 and P242C across the temperature range studied amounts to just one spin per molecule (Table S5). These data thus suggest that Fe−S cluster EPR signals from both native Hyd-1 and P242C arise from just one cluster (which must be the proximal cluster) and that the transformation of the spectrum of native Hyd-1 at low-potential is *not* due to two $S = 1/2$ species that relax at very different rates.

(2) W-band two-pulse echo-detected field sweeps of both reduced native Hyd-1 and P242C were conducted, and the resulting numerical derivative spectra are compared to the X-band CW spectra in Figure 3. The Fe−S EPR spectrum at X- and W-band in P242C is well described by a single rhombic g matrix ($g_{x,y,z}$ = 2.035, 1.923, 1.862) arising from the proximal cluster. Peaks observed for reduced native Hyd-1 at W-band at 3 K can also be well explained with just one rhombic g matrix ($g_{x,y,z}$ = 2.045, 1.916, 1.865). It is virtually impossible that we can be observing $S = 1/2$ spectra from two clusters.

(3) To search for the presence of clusters with $S \neq 1/2$ ground states, echo-detected EPR field-sweep spectra over a wide magnetic field range were conducted on concentrated low-potential samples of native Hyd-1 and the medial and proximal cluster variants (Figure 4). In all reduced Hyd-1 enzymes from several different sample preparations, broad peaks were observed up to ca. 800 mT at low temperatures (with a spin−lattice relaxation time <2 ms at 2.7 K). These broad signals must arise from the enzyme because hyperfine couplings to backbone ^{14}N nuclei could be detected (Figure S15). The data provide our most direct evidence for the presence of reduced Fe−S clusters with a $S > 1/2$ ground state.

(4) Like all [NiFe]-hydrogenases crystallized to date, the distal cluster is coordinated by three Cys residues and one His residue (Figure 1A). If the distal cluster contributes to the low-potential EPR spectrum of native Hyd-1 or the P242C variant (Figure 3), then it ought to be possible to detect the directly coordinating N of His187 via HYSCORE, as was shown for a pyridine inhibitor binding to the [4Fe-4S]$^+$ protein IspH (LytB) from *Aquifex aeolicus* (Aa IspH/inhibitor, see Table 2 for ^{14}N couplings).[43] However, exhaustive HYSCORE experiments with different pulse matchings, at different field positions, and with different τ values failed to detect any signals from a strongly coupled ^{14}N nucleus (Figure S16), thus providing indirect evidence that the reduced distal cluster does not have a $S = 1/2$ spin state.

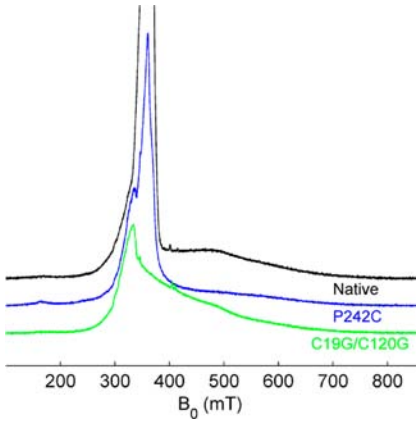

Figure 4. X-band two-pulse echo-detected wide field sweeps of native Hyd-1 and variants (2.7 K). Measurement conditions: pulse sequence $\pi/2-\tau-\pi-\tau-$echo, where τ is varied between 140 and 188 ns in 16 ns increments (to minimize distortions arising from nitrogen modulations) with $\pi/2$ = 16 ns; mw frequency 9.740 GHz (native, C19G/C120G), 9.745 GHz (P242C); shot repetition time 2 ms. The $g = 2$ region in native Hyd-1 and P242C was deliberately saturated. Sample conditions: −355 mV (native, H_2 reduced, 555 μM), −250 mV (P242C, dithionite reduced, approximately 300 μM), −200 mV (C19G/C120G, dithionite reduced, approximately 300 μM).

(5) We were unable to detect any electron−electron dipolar interaction between the proximal and distal clusters in H_2-reduced native Hyd-1 samples using DEER spectroscopy (see SI), consistent with the reduced distal cluster not having a $S = 1/2$ spin state.

(6) To probe the possibility that the distal and medial [4Fe−4S] clusters in Hyd-1 P242C have an $S = 1/2$ ground state but evade detection because they have very low reduction potentials, we employed an extremely powerful reducing agent, Eu(II)DTPA, to reach potentials well below those obtainable with either H_2 or sodium dithionite.[31] Figure 5 compares the 20 K CW EPR spectra of P242C reduced to −351 mV with H_2 and to −705 mV with 8 mol equiv of Eu(II)DTPA (under H_2, to inhibit H_2 production by the enzyme). Although the latter spectrum contains signals arising from Eu(II)-DTPA that has not been oxidized by the enzyme (cf. Eu(II)DTPA control, black line), it is clear that no additional Fe−S cluster CW EPR signals are present. Further Fe−S cluster CW EPR signals were not revealed at lower temperatures or at even more negative potentials, close to −0.9 V (Figure S9). The C19G/C120G/P242C variant, reduced to −796 mV with 8 mol equiv of Eu(II)DTPA under H_2, exhibits no EPR signals other than those attributable to Eu(II) (Figure S9). It is extremely unlikely that the imposition of such negative potentials (far lower than ought to be encountered in any physiological situation) could fail to reduce a sizable fraction of [4Fe−4S]$^{2+}$ clusters. The fact that we do not detect any new $S = 1/2$ EPR signals over such a wide potential range provides a strong argument that the reduced [4Fe−4S]$^+$ forms have higher spin states.

The redox states of the Fe−S clusters and the active site in Hyd-1 and its proximal and medial cluster variants, color-coded by their 'EPR visibility', are summarized in Figure 6 which

dx.doi.org/10.1021/ja307117y | J. Am. Chem. Soc. 2012, 134, 15581−15594

Table 2. Hyperfine and Nuclear Quadrupole Parameters for Nuclei N1 and N2 and Weakly Coupled $^{14}N_\varepsilon$ of His83 to the Active Site in *Ec* Hyd-1 P242C, Compared to Selected Parameters Reported in the Literature

sample/coupling	A (MHz)	A_{iso} (MHz)	T (MHz)	e^2qQ/h (MHz)	η	Fe−N bond length (Å)
N1 of P242C (Fe−S)	11.5,11.5,16.0[d]	13.0	−1.5,−1.5,3.0	–	–	2.1/2.2[17]
N2 of P242C (Fe−S)	2.8,4.6,3.5[e]	3.6	−0.8,1.0,−0.1	1.0	0	3.1
guanine N1/MoaA[70]	1.2,5.4,4.1	3.5	−2.3,1.9,0.6	−3.0	0	1.94[a]
Aa IspH/inhibitor[43]	6.2,7.6,8.4	7.4	−1.2,0.2,1.0	3.0	–	1.95[b]
N_{C20} of *Re*-MBH[69]	11.4, 14.1, 18.2	14.6	−3.2,−0.5,3.6	–	–	N/A[c]
N3 P242C (Ni−A/Ni−B)	2.0,2.3,2.3	2.2	−0.2,0.1,0.1	1.9	0.4	
Re-MBH (Ni−B)[22]	–	1.4−1.6	–	1.94	0.38	
Aa Hase I (Ni−C)[47]	1.22,1.33,2.07	1.54	−0.3,−0.2,0.5	1.92	0.40	
D. vulgaris (Ni−B)[22]	–	1.4−1.6	–	1.9	0.37	

[a]Distance in proposed modeled structure in ref 70. [b]This distance was calculated based on the quantum-mechanically geometry-optimized coordinates of the $[(Fe_4S_4)(SMe_4)_3(pyr)]^{2-}$ (model for IspH + inhibitor BPH-293) given in ref 43. [c]The crystal structure of the oxidized from of *Re*-MBH has not yet been published. [d]Error on each value ±1.5 MHz. [e]Error on each value ±0.3 MHz.

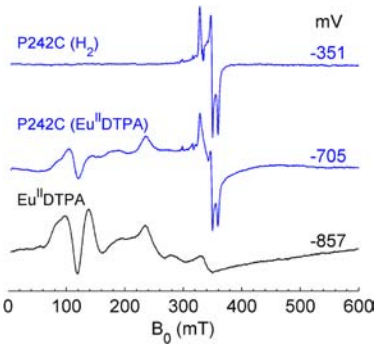

Figure 5. X-band CW EPR spectra of *Ec* Hyd-1 P242C, reduced to different potentials with H_2 or Eu(II)DTPA. Measurement conditions: mw power 0.5 mW; modulation amplitude 1 mT (all); 9.376 GHz (top), 9.371 GHz (middle), 9.370 GHz (bottom), 20 K. Sample concentration: 100 μM (P242C), EuDTPA (0.8 mM). The solution potentials were monitored via chronopotentiometry (Figure S8), and the potential values given are within ±2 mV.

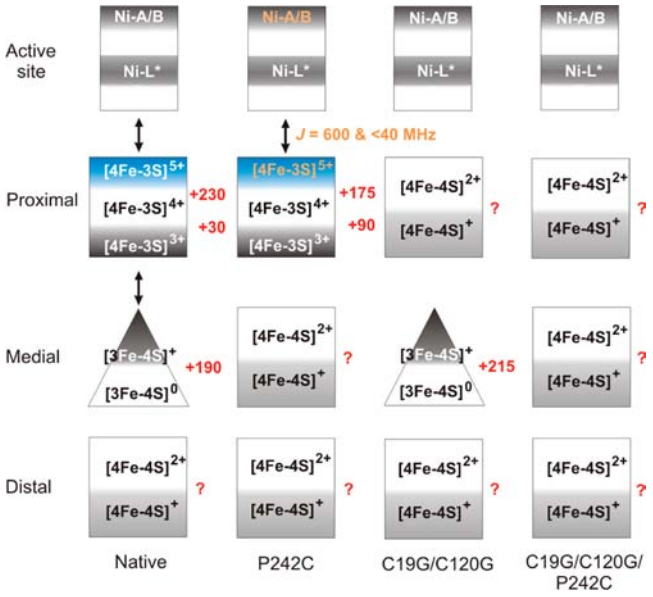

Figure 6. Cartoon summarizing the occurrence and EPR detectability of redox states of the Fe−S cluster relay and the active site in *Ec* Hyd-1 and variants. Included are reduction potentials and coupling parameters determined in this work. Redox states are colored as: dark gray (EPR visible), white (EPR silent), light gray (noninteger $S > 1/2$, but not detected by EPR), and blue (EPR active and of particular interest), and the cluster core charges are indicated. Double-headed arrows represent observed magnetic interactions between centers in EPR-visible redox states, and the exchange interactions (J) determined between the superoxidized proximal cluster and the active site for the P242C variant are shown in orange (Table 3). Reduction potentials (in mV) are given in red; a question mark indicates that the reduction potential of the particular redox transition is unknown.

includes the reduction potentials and exchange couplings (see below) that we have determined.

HYSCORE Investigations of the 'Superoxidized' Proximal Cluster. The nature of the Fe_4-N_{C20} bond and proximal $[4Fe-3S]^{5+}$ cluster at high potential (Figure 1B) was investigated in native Hyd-1 and P242C via HYSCORE. Figure 7Ai,ii shows two HYSCORE spectra of P242C measured at a field position where the Fe−S signal is intense (Figure S17). The spectra reveal single-quantum (sq) and double-quantum (dq) cross-peaks in the expected positions for two strongly coupled ^{14}N nuclei [with the strong coupling condition defined as $|A| > 2|\nu_{^{14}N}| \cong 2.15$ MHz, where peaks are most intense in the (−,+) quadrant]. In contrast, no cross-peaks that are easily assigned to ^{14}N are identifiable in the native enzyme (Figure S18). Similarly, ^1H cross-peaks are well-defined in P242C, but only a peak at the ^1H nuclear Zeeman frequency is observed in native Hyd-1. Further HYSCORE measurements at different field positions in the EPR spectra were therefore carried out with P242C, with the strongest coupling N1 only detected by matched HYSCORE experiments. Combined, these spectra (Figures S19 and S20) allowed three ^{14}N couplings to be determined; N1 and N2 are strongly coupled to the proximal $[4Fe-3S]^{5+}$ cluster, whereas N3 is weakly coupled to the active site [NiFe] center (Figure 7B). The spin Hamiltonian used to model the HYSCORE spectra and extract ^{14}N magnetic parameters is

$$H_{tot} = H_{ez}^{FeS} + H_{ez}^{Ni} + H_J + H_{nz} + H_{hf} + H_{nq} \quad (1)$$

The ^{14}N nuclear Zeeman (H_{nz}), hyperfine (H_{hf}), and nuclear quadrupole (H_{nq}) interactions are associated with either the proximal $[4Fe-3S]^{5+}$ cluster spin or the [NiFe] spin. Diagonalization of eq 1 to find the energy levels enabled the HYSCORE cross-peak positions to be calculated exactly; no peak intensities were calculated. In Figure 7Ai,ii, N1 and N2 are identifiable by their (dq,dq) cross-peaks which are sharp since they are broadened by the nuclear quadrupole interaction (NQI) only through second-order contributions. Hyperfine couplings for both N1 and N2 were principally obtained from the (dq,dq) cross-peaks recorded at different field positions

dx.doi.org/10.1021/ja307117y | J. Am. Chem. Soc. 2012, 134, 15581−15594

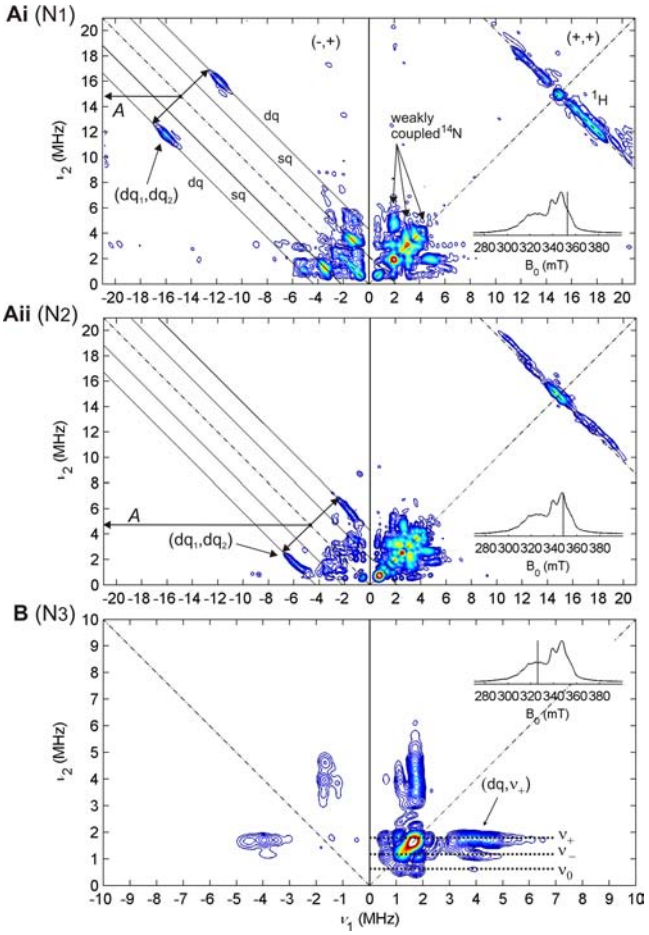

Figure 7. X-band HYSCORE spectra showing the three different ^{14}N nuclei (N1, N2 , and N3) observed in P242C at high potential. (Ai) Measurement at 352.8 mT exemplifying the cross-peaks observed from strongly coupled N1 assigned to N_{C20}. (Aii) Measurement at 348.2 mT exemplifying the cross-peaks observed from strongly coupled N2 assigned to N_{C19}. An estimate for the effective hyperfine couplings (A) for N1 and N2 can be determined by inspecting the dq transition cross-peaks (see also Figures S19–S21). (B) Measurement at 326.0 mT exemplifying the cross-peaks observed from weakly coupled N3 (in the exact cancellation condition) assigned to $^{14}N_\varepsilon$ of His 83 (see also Figures S19 and S22). Measurement conditions: (Ai) 9.728 GHz, 15 K, τ = 128 ns, matched pulses; (Aii and B) 9.737 GHz, 15 K, τ = 108 ns. Insets show the echo-detected field sweep spectra and the field positions for the HYSCORE measurements (vertical lines). Sample conditions: 622 μM, oxidized to +381 mV.

(Table 2). Initial estimates are readily made using the first-order equation for the dq nuclear frequencies:

$$\mathrm{dq}^{\alpha,\beta} \approx |A \mp 2\nu_{^{14}\mathrm{N}}| \tag{2}$$

where A is the hyperfine coupling, as indicated in Figures 7Ai,ii. Examination of the (dq,dq) cross-peak simulations as a function of J (Figure S21) for either N1 or N2 places an upper limit of J < 200 MHz on the exchange interaction between the proximal $[4Fe{-}3S]^{5+}$ cluster and the active site. Larger J values result in a resolved splitting in the simulations which is not observed experimentally. The sq signals for N1 were not detected, presumably because they are broadened to first order by the NQI and are therefore too weak to be observed (note that the dq peaks are weak and required matched pulses to be detected). The lack of observation of these peaks prevents the NQI from being determined. For N2, sq signals are observed, but it is difficult to identify all the expected peaks since they occur in a region of the HYSCORE spectrum (ca. ν_1,ν_2 < 5 MHz) where very intense peaks from weakly coupled 'free' peptide backbone nitrogens appear (e.g., from the hydrogen-bonded H229 ^{14}N in the vicinity of the proximal $[4Fe{-}3S]^{5+}$ cluster, Figure 1). Nonetheless, dq and sq peaks assigned to N2 allowed the NQI parameters to be estimated, and they are listed in Table 2.

The limit on the exchange coupling J obtained from the dq peaks of N1 and N2 in the HYSCORE spectra shows that a high-potential Fe–S species is present with a small exchange coupling to the active site. However, as stated above, the high potential X-band CW EPR spectra exhibit Ni–A and Ni–B signals that are split by a very large exchange coupling ($J \sim 600$ MHz) from the nearby $[4Fe{-}3S]^{5+}$ proximal cluster (Figure 2Ai). The HYSCORE and CW EPR data can thus only be interpreted if the high-potential Fe–S signals arise from at least two species. Simulations of the X- and W-band EPR data using a model comprising two high-potential EPR components, HP1 and HP2, are presented below (Figure 8).

The weakly coupled ^{14}N nucleus N3 clearly observed at low-field (Figure 7B) is assigned to N_ε of His83 hydrogen bonded to [NiFe]-μ-Cys549 (Figure 1) on the basis of previous investigations.[22,44−48] The exact cancellation condition ($|A| \cong 2|\nu^{14}_{\mathrm{N}}|$) is satisfactorily met for this nucleus at X-band, i.e., the hyperfine and nuclear Zeeman interactions cancel in one of the electron spin manifolds m_S. In this regime the three nuclear quadrupole frequencies are directly observed (ν_0, ν_-, and ν_+).[22,45,49] In Figure 7B the cross-peaks relating the ν_0, ν_-, and ν_+ transitions to the dq transition in the other 'noncanceled' m_S manifold are indicated, and these allow NQ parameters (e^2qQ/h and η) to be estimated from the principal values of the quadrupole tensor $\mathbf{P}_i$:[22,45,49,50]

$$P_1 = \frac{1}{3}(\nu_+ - 2\nu_-) = \frac{e^2qQ}{4h}(\eta - 1)$$

$$P_2 = \frac{1}{3}(\nu_- - 2\nu_+) = -\frac{e^2qQ}{4h}(\eta + 1)$$

$$P_3 = \frac{1}{3}(\nu_+ + \nu_-) = \frac{e^2qQ}{2h} \tag{3}$$

The dq transition occurring at

$$\nu^+_{\mathrm{dq}} = 2\left[\left(\nu_{^{14}\mathrm{N}} \pm \frac{|A|}{2}\right)^2 + \zeta^2\right]^{1/2},$$

$$\zeta = e^2qQ/4h(3+\eta^2)^{1/2} \tag{4}$$

yields an estimate of A.[22,45,49] However, exact frequency calculations using eq 1 were necessary to account for the exchange coupling J, and these establish an upper limit of J < 800 MHz (this HYSCORE spectrum has long peaks running parallel to the axes and any J splitting in this case would not be resolved until J gets very large, Figure S22). The insensitivity of the HYSCORE cross-peak positions for this nucleus to the magnitude of J explains why similar spectra and magnetic parameters have been reported for numerous different hydrogenases in both the reduced (catalytically active Ni species coupled to the reduced proximal $[4Fe{-}3S]^{3+}$ or $[4Fe{-}4S]^{+}$ cluster) and the oxidized (Ni–A and/or Ni–B coupled to proximal $[4Fe{-}3S]^{5+}$ in O_2-tolerant enzymes) states for which

dx.doi.org/10.1021/ja307117y | J. Am. Chem. Soc. 2012, 134, 15581−15594

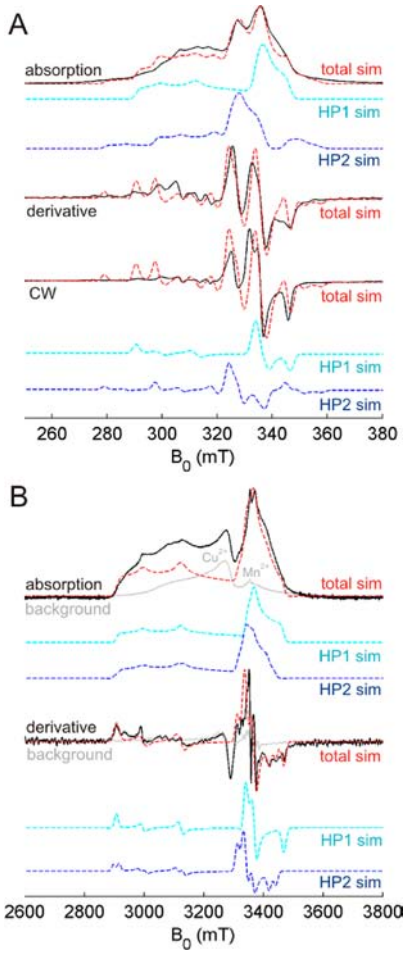

Figure 8. Simulation of EPR spectra of P242C poised at high potential in terms of a four-component model. (A) X-band echo-detected EPR (top, black), its derivative (middle, black), and CW EPR (bottom, black) spectra and their simulation; HP1−Ni−A + HP1−Ni−B (cyan), HP2−Ni−A + HP2−Ni−B (blue), and their total (red); HP1 and HP2 denote the two conformations of the proximal $[4Fe-3S]^{5+}$ cluster. Equal contributions of HP1 and HP2 are assumed, and the Ni−A:Ni−B ratio is 1:2 as determined by X-band CW EPR measurements at 125 K (Figure S10). (B) Corresponding W-band data. The first derivative experimental spectrum (bottom) was obtained by numerical differentiation of the absorption spectrum (top). The background spectra (gray) refer to a sample containing buffer only; note that the Cu^{2+} and Mn^{2+} peaks result from W-band probehead contaminations rather than impurities in the buffer (see Methods section). Measurement and sample conditions: (X-band): mw power 0.5 mW, modulation amplitude 1 mT, 20 K, 622 μM, +381 mV; (W-band) pulse sequence $\pi/2-\tau-\pi-\tau-$echo, where τ = 180 ns (P242C) or 220 ns (background), $t_{\pi/2}$ = 32 ns, t_{π} = 64 ns, shot repetition time 5 ms, mw frequency 93.855 GHz (P242C), 93.900 GHz (background), 3 K, 250 μM, approximately +373 mV. The P242C W-band sample was measured in the central region (g = 2.34−1.91) with more accumulations to improve the signal-to-noise. Simulation parameters are given in Table 3.

very different J couplings are reported.[22,45−47] Table 2 compares the N3 parameters to those previously reported for [NiFe]-hydrogenases, including the O_2-tolerant *Re*-MBH[22] and *Aquifex aeolicus* hydrogenase I (*Aa* Hase I).[47] A more extensive comparative set is provided in Table S6.

Model of the 'Superoxidized' P242C EPR Spectra. Figure 8 shows the experimental EPR spectra at X- (A) and W- (B) bands from P242C poised at high-potential, along with the simulations which comprise Ni−A and Ni−B coupled to two Fe−S species (conformers, see Discussion section) labeled HP1 and HP2; the exchange coupling scheme employed is HP1−Ni−A (J_{1A}) and HP1−Ni−B (J_{1B}) and HP2−Ni−A (J_{2A}) and HP2−Ni−B (J_{2B}), in which it is anticipated that $J_{1A} \approx J_{1B}$ and $J_{2A} \approx J_{2B}$. As shown in Table 3, HP1 has very small exchange

Table 3. The g Values for the Proximal $[4Fe-3S]^{5+}$ Cluster and Exchange Couplings with the Active Site in O_2-Tolerant [NiFe]-Hydrogenases

[NiFe]-hydrogenase	$[4Fe-3S]^{5+}$ g values (Euler angles, radians)	J (MHz)
Re-MBH[22]	$\approx g_e$	780 and 550[b]
Aa Hase I[14]	2.010, 2.015, 1.990	630
Native *Ec* Hyd-1[17]	2.043, 2.031, 2.007	–
P242C HP1[a]	2.008, 1.990, 1.933 (2.36, 0.79 2.36)	<40 (J_{1A} & J_{1B})
P242C HP2[a]	2.000, 1.955, 2.018 (0.79, 1.57, 2.36)	600 (J_{2A} & J_{2B})

[a]Simulation parameters for Ni−A: $g_{x,y,z}$ = 2.31, 2.24, 2.01; Euler angles (−2.81, 2.30, 2.41) radians and Ni−B: $g_{x,y,z}$ = 2.31, 2.15, 2.01; Euler angles (−2.81, 2.30, 2.41) radians; Euler angles were based on ref 79. $J_{1A/B}/J_{2A/B}$ designate the exchange couplings between Ni−A/Ni−B and HP1/HP2, respectively (Figure 8 and Figure S21). The simulations included an electron dipole−dipole interaction between each HP and [NiFe] pair, with the unique principal value axis taken to be directed between the two centers with a coupling of (−17,−17, +34) MHz. This coupling was determined using coordinates from ref 17 (PDB 3USC) in conjunction with the point-dipolar model, employing a S = 1/2 spin for the [NiFe] site and using the four spin projection factors listed in ref 17 to model the Fe−S spin. The g values and Euler angles for HP1 and HP2 are given for our best simulation but are not unique. [b]The two exchange couplings J belong to one spin system where Ni−B is coupled to two X^{ox} species.[22]

couplings to both Ni−A and Ni−B, and nitrogen nuclei N1 and N2 detected by HYSCORE are thus assigned to HP1. Conformer HP2 has large exchange couplings to the active site, and this gives rise to the observed signals at X-band which are considerably shifted from their g-value resonant positions. Figure 8 presents both absorption and first harmonic (or first derivative) representations and simulations for the individual components and their sum. These simulations convincingly demonstrate that a four-component model is able to account for the data. The experimental spectral width and intensity at both mw frequencies is well described; note that the weak spectral wings apparent in the X- and W-band absorption spectra are modeled. In further support of the model is the lack of cross-peaks from N1 in HYSCORE spectra measured at the low-field side of the Fe−S EPR spectrum (Figure S20) where the EPR simulations predict that only HP2 is present. The detailed information obtained from the simulations is made possible by the P242C variant, which removes the exchange couplings to the medial cluster present in native Hyd-1. Exhaustive efforts to simulate the EPR data with only one Fe−S paramagnetic center were unsuccessful.[51]

DISCUSSION

The reduction potential of the $[4Fe-3S]^{5+/4+}$ couple in native Hyd-1 is similar to those determined for *Aa* Hase I[14] and the [NiFe]-hydrogenase from *R. metallidurans*, while that for *Re*-MBH was reported to be considerably less positive[23] and closer in value to that found for the medial cluster P242C variant of *Ec* Hyd-1 (Table 1). Although the structure and electronic nature of the cluster should be very similar for all these enzymes, the

dx.doi.org/10.1021/ja307117y | J. Am. Chem. Soc. 2012, 134, 15581−15594

electrostatic environment is likely to vary depending on the amino acid sequence beyond residues directly ligating the proximal cluster, thus affecting its reduction potential. In particular, given the distance between the proximal cluster and P242 (~13 Å), it is not surprising that the reduction potentials are affected by the P242C mutation at the medial cluster. The reduction potentials of the $[3Fe-4S]^{+/0}$ couple in native Hyd-1 and the proximal cluster C19G/C120G variant differ slightly but are within experimental error (Table 1). Notably, in native Hyd-1 the medial $[3Fe-4S]^{0}$ cluster is almost as reducing as the proximal $[4Fe-3S]^{4+}$ cluster. This leveling of the $[3Fe-4S]^{+/0}$ and $[4Fe-3S]^{5+/4+}$ reduction potentials is also likely to be the case for the native O_2-tolerant hydrogenases from *Aa* Hase I, *Re*-MBH and *Rm* CH34, but because the midpoint potentials determined for the medial cluster were 'apparent' values, the true midpoint was hidden. Measurement of the medial cluster's midpoint potential is uncomplicated for the C19G/C120G variant. It would be informative to see how the medial cluster $[3Fe-4S]^{+/0}$ reduction potential of the same variant in *Re*-MBH[11] compares. The high reduction potential of the medial $[3Fe-4S]^{+/0}$ cluster in O_2-tolerant hydrogenases suggests that this center also plays an essential role in ensuring the formation of the harmless Ni–B state when O_2 attacks the active site. Four electrons are required to fully reduce O_2 (and form Ni–B), of which two are now known to be provided by the proximal cluster.[10,11,13,14,16,17] The active site can automatically provide one electron if it starts from its most oxidized active state (Ni–SI, formally containing Ni(II)),[52] in which case we hypothesize that the fourth electron originates from the medial cluster. Since the medial cluster in the P242C variant does not exhibit $S = 1/2$ EPR signals between +0.4 and −0.9 V (Figure 5, Figures S3 and S9), we were unable to determine its reduction potential. However, assuming it is a [4Fe–4S] cluster, its reduction potential should be more negative than the [3Fe–4S] cluster in native Hyd-1, and therefore less effective at holding an electron. Electrochemical studies to investigate the O_2 tolerance of P242C are underway.

The reduced Ni species in all Hyd-1 enzymes are significantly different to both standard and O_2-tolerant enzymes from other species; specifically, we could not detect the Ni–C state which contains a Ni(III)–H^- motif[53] and is thought to be an intermediate in the catalytic cycle, one electron equivalent more reduced than Ni–SI. The state known as Ni–L is normally formed from Ni–C upon illumination at low temperature.[53] The exact structure of Ni–L remains elusive, but the bound hydride in Ni–C is thought to dissociate as H^+ and bind to a nearby base, leaving the bridging site empty with Ni(III) formally reduced to Ni(I).[52] However, the Ni–L* species observed in Hyd-1 (see Figure 2 and Figure S12) is similar to the Ni–L1 state of *Aa* Hase I[47] detected in CW EPR spectra at 70 K, and in each case, both are formed without illumination. A pure Ni–C species in *Aa* Hase I could only be induced at 100 K in the dark,[47] suggesting that in this enzyme the energy barrier for the conversion of Ni–L to Ni–C is lower than in standard hydrogenases. In support of this hypothesis, Pandelia et al.[47] reported that Ni–C of *Aa* Hase I contains a more weakly bound hydride. Several arguments point toward a structural similarity of Hyd-1 Ni–L* with Ni–L rather than Ni–C. First, the *g* values are similar to the light-induced state Ni–L2 of *Desulfomicrobium baculatum* [NiFeSe]-hydrogenase[55] and the Ni–L1 state of *Aa* Hase I.[47] Second, the splitting pattern due to magnetic interaction with the reduced proximal cluster (Figure 2Aiv) is similar to that of Ni–L in hydrogenases from other species[54] but different to that of Ni–C.[55] Lill and Siegbahn[56] recently proposed a catalytic cycle for [NiFe]-hydrogenases based on theoretical calculations which includes the Ni–L state: with Hyd-1 we therefore provide experimental evidence that Ni–L may not be an artifact induced by light.

The X-band CW EPR spectra of native Hyd-1, *Re*-MBH and *Aa* Hase I at various potentials are strikingly similar, as are those of the C19G/C120G *Ec* Hyd-1 and *Re*-MBH variants.[11,14,15] This relationship may be expected since sequence alignments and crystal structures of as-isolated enzymes show that the cofactor arrangement and their ligation are highly conserved. Nonetheless, contrary to what has been proposed for *Aa* Hase I, we conclude (as summarized above) that the distal cluster $[4Fe-4S]^{+}$ does not contribute to the low-potential Fe–S cluster EPR signals detected in native Hyd-1 and assigned to a $S = 1/2$ system. On the basis of all our evidence we propose that the low-potential complex interaction signal observed in O_2-tolerant hydrogenases arises from the reduced proximal cluster ($S = 1/2$) coupled to the medial $[3Fe-4S]^{0}$ cluster ($S = 2$).[27] The temperature dependence of the X-band CW EPR spectra (Figure 3) may be due to an exchange interaction between the proximal and medial clusters which is modulated as a function of temperature by a change in the T_1 relaxation time of the medial cluster ($S = 2$). The fact that the W-band spectrum has no resolved exchange splitting suggests that the exchange coupling is less than the W-band line width of ca. 700 MHz, a feasible upper limit given the spacing between the turning points in the X-band EPR spectra. Since the reduced medial cluster parameters are unknown, this interpretation cannot currently be verified through simulation of the CW EPR data. The titration data of native Hyd-1 show that the shape of the complex interaction signal observed clearly below ca. 30 mV changes not only with temperature (Figure 3) but also (more subtly) with potential (Figure 2, Figure S2). This temperature and potential dependence is also apparent in titrations of *Aa* Hase I.[14] However, in the medial cluster P242C variant the appearance of the rhombic *g* matrix is unaffected by both temperature and potential (Figure 2, Figures S3 and S14). It is thus likely that the slight change in shape of the native Hyd-1 signals below ca. 30 mV is due to the completion of the $[3Fe-4S]^{+/0}$ redox transition as the potential is lowered (Figure 2).

High-spin ground states in reduced [4Fe–4S] clusters are well documented,[57−60] and it should not be surprising that the distal cluster in some O_2-tolerant [NiFe]-hydrogenases have a ground state $S \neq 1/2$. Studies of small synthetic analogues by no means show that $S = 1/2$ ground states are the norm for reduced [4Fe–4S] clusters.[57−60] The [4Fe–4S] cluster in the hydrogenase subunit of the NAD^+-reducing [NiFe]-hydrogenase from *Ralstonia eutropha*, proposed to have all-cysteine ligation, could not be detected by EPR when reduced with dithionite or H_2.[61] Although the factors leading to high-spin ground states in $[4Fe-4S]^{+}$ clusters are not very well understood, mutation of one of the cysteines in an all Cys-ligated $[4Fe-4S]^{+}$ cluster with a ground state $S = 1/2$ has previously been demonstrated to lead to a higher spin state,[62] and high-spin $[4Fe-4S]^{+}$ clusters reported in the literature are typically ligated by three Cys residues and one different amino acid. Examples include the FS0 cluster in nitrate reductase (ligated by three Cys and one His),[63] the 'labile' [4Fe–4S] cluster in *Desulfovibrio africanus* ferredoxin III,[64,65] and the [4Fe–4S] cluster in *Pyrococcus furiosus* ferredoxin[66] (both ligated by three Cys and one Asp). The ligation of the cluster in

dx.doi.org/10.1021/ja307117y | J. Am. Chem. Soc. 2012, 134, 15581−15594

the latter protein has been extensively studied,[67] and in a D14C variant, the $[4Fe-4S]^{+}$ cluster was found to be exclusively in the $S = 1/2$ ground state. Similarly, the 'labile' $[4Fe-4S]^{+}$ cluster in ferredoxin III from *D. africanus* also changed from an $S = 3/2$ ground state in the native protein to a $S = 1/2$ ground state in the D14C variant.[65] Given that the reduced Fe−S cluster signals in O_2-tolerant [NiFe]-hydrogenases are much better defined compared to standard [NiFe]-hydrogenases,[11,14,15] it may be possible to investigate the Fe−S cluster signals in distal cluster variants of Hyd-1 in more detail than was previously possible with distal cluster variants of the standard [NiFe]-hydrogenase from *D. fructosovorans*.[68] The finding that the reduced distal cluster in *Ec* Hyd-1 (and perhaps many more [NiFe]-hydrogenases) has a high-spin ground state reinforces the need to search for these elusive spin-states in many other enzymes containing Fe−S clusters.

The X- and W-band EPR and X-band HYSCORE data of the P242C variant poised at high potential (Figure 8) clearly show that two different conformations of the proximal $[4Fe-3S]^{5+}$ cluster are present, a result which is fully consistent with the crystal structure data for the native enzyme revealing two conformations for the $[4Fe-3S]^{5+}$ cluster,[17] which oscillates between E76 and C19 shifting its position by 0.7 Å, as shown in Figure 1B. The presence of two paramagnetic conformers of the superoxidized proximal cluster reinforces its dynamic nature, and our EPR studies indicate that conformer HP2 has a strong electronic pathway to the active site, whereas HP1 is by comparison relatively electronically "insulated". Confidence in the EPR model and the magnetic parameters is only made possible because the P242C variant eliminates the couplings to the medial cluster $[3Fe-4S]^{+}$ paramagnet. X-band HYSCORE cross-peaks from strongly coupled ^{14}N nuclei are sensitive to the exchange interaction which allows the nitrogen nuclei N1 and N2 to be assigned to conformer HP1. We were unable to detect any strongly coupled ^{14}N signal from HP2 with our experiments, presumably a result of fast relaxation due to the presence of the strong exchange interaction. Note that HYSCORE experiments on native Hyd-1 also failed to detect any strong ^{14}N couplings or ^{1}H couplings >1 MHz which must be present, presumably also because of the large exchange interaction with the medial cluster and resultant fast relaxation. Experiments at higher mw frequencies may be able to mitigate this relaxation problem.[22,69] The presence of two conformers of the proximal cluster, which cannot have exactly the same physical properties, offers an explanation for why the potentiometric titrations for P242C show a field dependence of the $[4Fe-3S]^{5+/4+}$ couple (Figures S3 and S6B).

The magnetic parameters for N1 and N2 are summarized in Table 2 and compared to data reported for Fe−N bonds in three other Fe−S systems: the nitrogen of a guanine substrate binding to a $[4Fe-4S]^{+}$ cluster of the S-adenosyl-methionine-dependent enzyme MoaA (guanine N1/MoaA);[70] a pyridine inhibitor binding to the $[4Fe-4S]^{+}$ protein IspH *Aa* IspH/inhibitor;[43] and the proximal cluster in *Re*-MBH, for which recent $^{14/15}N$ Q-band ENDOR data were assigned to the amide nitrogen coordinating Fe_4 (also Fe_4 in *Re*-MBH)—to our knowledge, the first EPR data presented for the Fe−N bond in the superoxidized cluster in an O_2-tolerant [NiFe]-hydrogenase.[69] The largest coupling N1 can be unambiguously assigned to N_{C20} since it is covalently bonded to Fe_4 (Fe_4-N_{C20} = 2.1 Å, Table 2); Fe_4 carries a large spin density, and thus a transfer of spin density to the N_{C20} orbitals gives rise to the large experimental hyperfine coupling. This coupling can be separated into an isotropic and an anistropic part:

$$(A_1, A_2, A_3) = A_{iso} + (-T, -T, 2T) \tag{5}$$

where the anisotropy of the hyperfine coupling is axial within experimental error (Table 2). Using the N1 coupling in Table 2 yields A_{iso} = 12.5−13.5 MHz and T = 0.5−2.5 MHz. The isotropic hyperfine coupling characterizes the s-orbital nature of the Fe_4-N_{C20} bond via the fraction of spin density f_{2s} residing in the 2*s* orbital of N_{C20}, which can be estimated from

$$f_{2s} = a_{iso} 2S / a^{0}_{2s} \tag{6}$$

where $a^{0}_{2s} \cong 1811$ MHz is the coupling for unit spin density in a nitrogen 2s orbital[71] and $S = 5/2$ for Fe^{3+}. The fundamental hyperfine coupling matrix **a** describes the interaction of the nitrogen with the spin of the isolated Fe^{3+} ion and is related to the experimental hyperfine coupling matrix **A** using the spin projection factor k derived from the spin-coupling model:[72,73]

$$\mathbf{A} = k\mathbf{a} \tag{7}$$

An estimate of the spin projection factors of the high-potential proximal cluster irons are reported in ref 17; $k_1 = -88/81$; $k_2 = +10/9$; $k_3 = -110/81$; $k_4 = +7/3$, where Fe_4 is formally assigned the 3+ oxidation state. Consequently, with A_{iso} = 12.5−13.5 MHz and $k_4 = 7/3$, eqs 6 and 7 yield a_{iso} = 5.36−5.79 MHz and f_{2s} = 1.5−1.6%. A similar value of $f_{2s} \sim 3\%$ was found for the histidine nitrogen coordinating Fe^{3+} ($S = 5/2$) in aquometmyoglobin.[74]

The anisotropic part of the hyperfine coupling consists of a direct dipolar coupling to the Fe−S cluster spin, and a local part due to nitrogen p-orbital spin density, $\mathbf{T} = \mathbf{T}_{dip} + \mathbf{A}_p$. The dipolar part $\mathbf{T}_{dip}$ would be expected to be large since N_{C20} is very close to the paramagnetic cluster and, in particular, subsite Fe_4 with a large spin projection factor. This contribution can be estimated using the point-dipolar formula:

$$\mathbf{T}_{dip} = \frac{\mu_0 \beta_e \beta_N g_e g_N}{4\pi h} \sum_j k_j \frac{3\mathbf{n}_j \mathbf{n}_j^{\dagger} - 1}{r_j^3} \tag{8}$$

where $\mathbf{T}_{dip}$ is the dipolar matrix, $\mathbf{n}_j$ and r_j are the nitrogen (k_j of Fe_j) unit row vector and distance, respectively, and † indicates a transpose. Substituting the four k_i values into eq 8 yields a dipolar matrix with principal values of [−1.6, −1.6, 3.2] MHz, where the unique axis (with principal value $2T_{dip}$ = 3.2 MHz) points essentially along the Fe_4-N_{C20} vector. This result is consistent with the size of the anisotropy observed experimentally (eq 5, mean anisotropic coupling [−1.5, −1.5, 3.0] MHz) and thus the 3+ assignment of the Fe_4 oxidation state.

Any remaining anisotropy is due to p-orbital spin density and should be small, as is now discussed. The crystal structure reveals that the N_{C20} bond angle ∠CNC = 119.4° (for both conformers), which suggests a sp^n hybrid orbital bonding scheme with $n \sim 2$. In such a case, the ratio f_{2p}/f_{2s} is ~2, where f_{2p} is the p-orbital spin density (for sp^2: $f_{2p}/f_{2s} = 2$ with ∠CNC = 120°).[74,75] It is thus instructive to make an estimate of the p-orbital spin density from the experimental hyperfine coupling to check that it is consistent with this expectation. The hyperfine coupling due to a p-orbital contribution can be estimated if we assume an axial experimental hyperfine interaction where the unique axis points along the Fe_4-N_{C20} vector with value $A_{iso} + 2T_{dip} + 2A_p$ (this implies a σ-orbital

contribution, and that the π-orbital contribution is small). The spin density in the p-orbital is then given by

$$f_{2p} = a_p 2S/a^0_{2p} \quad (9)$$

where $a^0_{2p} \cong 55$ MHz is the coupling for unit spin density in a nitrogen 2p orbital.[71] With a_p = 0−0.38 MHz, f_{2p} = 0−3.5% (excluding negative a_p values). Recalling that f_{2s} = 1.5−1.6%, it can be concluded that within error the experimental ratio is consistent with $f_{2p}/f_{2s} \sim 2$. Our approximate hyperfine coupling analysis is thus in accord with the expected p- and s-orbital contributions for a sp^n hybrid orbital picture, where the spin density predominately resides in a σ-orbital.

The second largest coupling N2 is assigned to N_{C19}, which is approximately 3.1 Å from Fe_4,[17] and using eq 8 leads to T_{dip} = [−0.6,−0.4,1.0] MHz, which compares favorably with the experimental values for N2 given in Table 2. Because HYSCORE data place an upper limit on the exchange coupling of $J \lesssim 200$ MHz for the paramagnetic center coupled to N2 (see Figure S21), it cannot be assigned to conformer HP2. Our assignment of N1 (N_{C20}) and N2 (N_{C19}) is consistent with Fe_4 being in the 3+ oxidation state and the spin coupling scheme and spin projection factors k_j given in ref 17, i.e., with k_4 around +7/3. The nitrogen hyperfine couplings to the [4Fe−4S]$^+$ clusters reported in refs 43 and 70 are significantly smaller than N1 (see Table 2), even though the N atom is also coordinated to a Fe of the cluster. The small dipolar part of the ^{14}N hyperfine coupling in these cases is likely due to the small spin projection factors which is estimated to be $k < |1.5|$ for Fe^{2+} or $Fe^{2.5+}$ in the 'normal' reduced ferredoxin-type [4Fe−4S]$^+$ clusters[72] found in guanine N1/MoaA and *Aa* IspH/inhibitor.

In summary, we have carried out a detailed study of the Fe−S relay in an O_2-tolerant [NiFe]-hydrogenase along with medial and proximal cluster variants, providing conclusive evidence that the distal cluster in the variants, and almost certainly also in the native enzyme, does not have a spin S = 1/2 ground state, thus precluding any straightforward measurement of its reduction potential. These observations have wider relevance for large Fe−S containing enzymes in general, where some sites may evade detection. Indeed, the Fe−S clusters in the Hyd-1 C19G/C120G/P242C variant are almost completely EPR silent (Figure 6). The medial [3Fe−4S]$^{+/0}$ cluster has a very positive reduction potential that may also assist O_2 tolerance. The P242C variant has proved to be extremely useful in resolving the properties of the superoxidized proximal cluster. We have shown that two conformations, already revealed in the crystal structure of native Hyd-1, have strikingly different exchange couplings to the active site. We have also shown, experimentally, that a localized Fe(III) subsite is produced upon superoxidation as a result of a rearrangement that generates a bond between that Fe and a deprotonated peptide nitrogen, a strong π-donor. The striking similarity of the oxidized and reduced forms of the nitrogenase P-cluster[16,76,77] with the proximal cluster found in O_2-tolerant hydrogenases[16,17] entails that mechanistic details revealed for the latter might provide important mechanistic clues for the mechanism of N_2 fixation by nitrogenase.

■ ASSOCIATED CONTENT

Supporting Information

Production and engineering of *Ec* Hyd-1 enzymes, solution activity assays, details for preparation of Eu(II)DTPA-reduced samples, supporting figures and tables. This information is available free of charge via the Internet at http://pubs.acs.org.

■ AUTHOR INFORMATION

Corresponding Author

jeffrey.harmer@chem.ox.ac.uk; fraser.armstrong@chem.ox.ac.uk

Notes

The authors declare no competing financial interest.

■ ACKNOWLEDGMENTS

This research was supported by the Engineering and Physical Sciences Research Council (grant EP/D044855D/1, supporting the Oxford Center for Advanced Electron Spin Resonance, CAESR) and by the Biological and Biotechnological Sciences Research Council (grants BB/H003878-1 and BB/I022309-1). We thank Dr. Michael Lukey for constructing the *Ec* Hyd-1 P242C variant, and Prof. Juan Fontecilla-Camps, Dr. Anne Volbeda, and Prof. David Collison for helpful discussions. Elena Nomerotskaia is gratefully acknowledged for help with protein purification. We also thank the National EPR Research Facility & Service in Manchester, and Daniel Sells and Dr. Floriana Tuna for valuable technical assistance.

■ REFERENCES

(1) Vignais, P. M.; Billoud, B. *Chem. Rev.* **2007**, *107*, 4206.
(2) Jones, A.; Sillery, E.; Albracht, S.; Armstrong, F. *Chem. Commun.* **2002**, 866.
(3) Fontecilla-Camps, J.; Volbeda, A.; Cavazza, C.; Nicolet, Y. *Chem. Rev.* **2007**, *107*, 4273.
(4) Volbeda, A.; Charon, M.-H.; Piras, C.; Hatchikian, C.; Frey, M.; Fontecilla-Camps, J. *Nature* **1995**, *373*, 580.
(5) Lanciano, P.; Savoyant, A.; Grimaldi, S.; Magalon, A.; Guigliarelli, B.; Bertrand, P. *J. Phys. Chem. B* **2007**, *111*, 13632.
(6) Dobbek, H.; Svetlitchnyi, V.; Gremer, L.; Huber, R.; Meyer, O. *Science* **2001**, *293*, 1281.
(7) Bertero, M.; Rothery, R.; Palak, M.; Hou, C.; Lim, D.; Blasco, F.; Weiner, J.; Strynadka, N. *Nat. Struct. Mol. Biol.* **2003**, *10*, 681.
(8) Sazanov, L.; Hinchliffe, P. *Science* **2006**, *311*, 1430.
(9) Page, C.; Moser, C.; Chen, X.; Dutton, L. *Nature* **1999**, *402*, 47.
(10) Fritsch, J.; Scheerer, P.; Frielingsdorf, S.; Kroschinsky, S.; Friedrich, B.; Lenz, O.; Spahn, C. M. T. *Nature* **2011**, *479*, 249.
(11) Goris, T.; Wait, A. F.; Saggu, M.; Fritsch, J.; Heidary, N.; Stein, M.; Zebger, I.; Lendzian, F.; Armstrong, F. A.; Friedrich, B.; Lenz, O. *Nat. Chem. Biol.* **2011**, *7*, 310.
(12) Lukey, M. J.; Parkin, A.; Roessler, M. M.; Murphy, B. J.; Harmer, J.; Palmer, T.; Sargent, F.; Armstrong, F. A. *J. Biol. Chem.* **2010**, *285*, 3928.
(13) Lukey, M. J.; Roessler, M. M.; Parkin, A.; Evans, R. M.; Davies, R. A.; Lenz, O.; Friedrich, B.; Sargent, F.; Armstrong, F. A. *J. Am. Chem. Soc.* **2011**, *133*, 16881.
(14) Pandelia, M.-E.; Nitschke, W.; Infossi, P.; Giudici-Orticoni, M.-T.; Bill, E.; Lubitz, W. *Proc. Natl. Acad. Sci. U.S.A.* **2011**, *108*, 6097.
(15) Saggu, M.; Zebger, I.; Ludwig, M.; Lenz, O.; Friedrich, B.; Hildebrandt, P.; Lendzian, F. *J. Biol. Chem.* **2009**, *284*, 16264.
(16) Shomura, Y.; Yoon, K.-S.; Nishihara, H.; Higuchi, Y. *Nature* **2011**, *479*, 253.
(17) Volbeda, A.; Amara, P.; Darnault, C.; Mouesca, J.-M.; Parkin, A.; Roessler, M. M.; Armstrong, F. A.; Fontecilla-Camps, J. C. *Proc. Natl. Acad. Sci. U.S.A.* **2012**, *109*, 5305.
(18) Friedrich, B.; Fritsch, J.; Lenz, O. *Curr. Opin. Biotechnol.* **2011**, *22*, 358.
(19) Parkin, A.; Sargent, F. *Curr. Opin. Chem. Biol.* **2012**, *16*, 26.
(20) Volbeda, A.; Martin, L.; Cavazza, C.; Matho, M.; Faber, B.; Roseboom, W.; Albracht, S.; Garcin, E.; Rousset, M.; Fontecilla-Camps, J. *J. Biol. Inorg. Chem.* **2005**, *10*, 239.

(21) Cracknell, J. A.; Wait, A. F.; Lenz, O.; Friedrich, B.; Armstrong, F. A. *Proc. Natl. Acad. Sci. U.S.A.* **2009**, *106*, 20681.
(22) Saggu, M.; Teutloff, C.; Ludwig, M.; Brecht, M.; Pandelia, M.-E.; Lenz, O.; Friedrich, B.; Lubitz, W.; Hildebrandt, P.; Lendzian, F.; Bittl, R. *Phys. Chem. Chem. Phys.* **2010**, *12*, 2139.
(23) Knuettel, K.; Schneider, K.; Erkens, A.; Plass, W.; Mueller, A.; Bill, E.; Trautwein, A. X. *Bull. Pol. Acad. Sci., Chem.* **1994**, *42*, 495.
(24) Schneider, K.; Patil, D.; Cammack, R. *Biochim. Biophys. Acta, Protein Struct. Mol. Enzymol.* **1983**, *748*, 353.
(25) Rousset, M.; Montet, Y.; Guigliarelli, B.; Forget, N.; Asso, M.; Bertrand, P.; Fontecilla-Camps, J. C.; Hatchikian, E. C. *Proc. Natl. Acad. Sci. U.S.A.* **1998**, *95*, 11625.
(26) Pershad, H.; Duff, J.; Heering, H.; Duin, E.; Albracht, S.; Armstrong, F. *Biochemistry* **1999**, *38*, 8992.
(27) Teixeira, M.; Moura, I.; Xavier, A. V.; Moura, J. J.; LeGall, J.; DerVartanian, D. V.; Peck, H. D.; Huynh, B. H. *J. Biol. Chem.* **1989**, *264*, 16435.
(28) Roberts, L.; Lindahl, P. *Biochemistry* **1994**, *33*, 14339.
(29) Teixeira, M.; Moura, I.; Xavier, A.; Hanh, H.; DerVartanian, D.; Peck, H.; LeGall, J.; Moura, J. *J. Biol. Chem.* **1985**, *260*, 8942.
(30) Patil, D. S.; Moura, J. J.; He, S. H.; Teixeira, M.; Prickril, B. C.; DerVartanian, D. V.; Peck, H. D.; LeGall, J.; Huynh, B. H. *J. Biol. Chem.* **1988**, *263*, 18732.
(31) Vincent, K. A.; Tilley, G. J.; Quammie, N. C.; Streeter, I.; Burgess, B. K.; Cheesman, M. R.; Armstrong, F. A. *Chem. Commun.* **2003**, 2590.
(32) Lee, C. C.; Hu, Y.; Ribbe, M. W. *Proc. Natl. Acad. Sci. U.S.A.* **2012**, *109*, 6922.
(33) Lee, C. C.; Hu, Y.; Ribbe, M. W. *Angew. Chem., Int. Ed.* **2012**, *51*, 1947.
(34) Danyal, K.; Inglet, B. S.; Vincent, K. A.; Barney, B. M.; Hoffman, B. M.; Armstrong, F. A.; Dean, D. R.; Seefeldt, L. C. *J. Am. Chem. Soc.* **2010**, *132*, 13197.
(35) Reda, T.; Barker, C.; Hirst, J. *Biochemistry* **2008**, *47*, 8885.
(36) Bernhard, M.; Benelli, B.; Hochkoeppler, A.; Zannoni, D.; Friedrich, B. *Eur. J. Biochem.* **1997**, *248*, 179.
(37) Nivière, V.; Hatchikian, E. C.; Bianco, P.; Haladjian, J. *Biochim. Biophys. Acta, Bioenerg.* **1988**, *935*, 34.
(38) Hexter, S.; Grey, F.; Happe, T.; Climent, V.; Armstrong, F. *Proc. Natl. Acad. Sci. U.S.A.* **2012**, *109*, 11516.
(39) Bradford, M. M. *Anal. Biochem.* **1976**, *72*, 248.
(40) Hofbauer, W.; Bittl, R. *J. Magn. Reson.* **2000**, *147*, 226.
(41) Casadaban, M. J.; Cohen, S. N. *Proc. Natl. Acad. Sci. U.S.A.* **1979**, *76*, 4530.
(42) Dubini, A.; Pye, R. L.; Jack, R. L.; Palmer, T.; Sargent, F. *Int. J. Hydrogen Energy* **2002**, *27*, 1413.
(43) Wang, W.; Li, J.; Wang, K.; Smirnova, T. I.; Oldfield, E. *J. Am. Chem. Soc.* **2011**, *133*, 6525.
(44) Brecht, M.; Stein, M.; Trofanchuk, O.; Lendzian, F.; Bittl, R.; Higuchi, Y.; Lubitz, W. *Magnetic Resonance and Related Phenomena*; Ziessow, D., Lendzian, F., Lubitz, W., Eds.; Technische Universität, Berlin: Berlin, 1998; pp 818−810.
(45) Buhrke, T.; Brecht, M.; Lubitz, W.; Friedrich, B. *J. Biol. Inorg. Chem.* **2002**, *7*, 897.
(46) Chapman, A.; Cammack, R.; Hatchikian, C. E.; McCracken, J.; Peisach, J. *FEBS Lett.* **1988**, *242*, 134.
(47) Pandelia, M.-E.; Infossi, P.; Stein, M.; Giudici-Orticoni, M.-T.; Lubitz, W. *Chem. Commun.* **2012**, *48*, 823.
(48) Roessler, M. M. Ph.D. Thesis, University of Oxford, Oxford, U.K., 2012.
(49) Foerster, S.; Gastel, M. v.; Brecht, M.; Lubitz, W. *J. Biol. Inorg. Chem.* **2005**, *10*, 51.
(50) Dikanov, S. A.; Tsvetkov, Y. *Electron Spin Echo Envelope Modulation (ESEEM)*; CRC Press: Boca Raton, FL, 1992.
(51) Not only could we not detect N1 signals (nor any other strongly coupled nitrogen nuclei) in the HYSCORE spectra recorded at the field positions where only HP2 is present but also no proton signals besides the matrix line are present either (Figure S20). These HYSCORE spectra resemble the behavior observed for native Hyd-1 where a large exchange coupling, presumably with the medial $[3Fe-4S]^{+}$ cluster, prevents detection of the coupled nearby nuclei (Figure S18).
(52) Lubitz, W.; Reijerse, E.; van Gastel, M. *Chem. Rev.* **2007**, *107*, 4331.
(53) Brecht, M.; van Gastel, M.; Buhrke, T.; Friedrich, B.; Lubitz, W. *J. Am. Chem. Soc.* **2003**, *125*, 13075.
(54) Medina, M.; Hatchikian, E. C.; Cammack, R. *Biochim. Biophys. Acta, Bioenerg.* **1996**, *1275*, 227.
(55) Bertrand, P.; Camensuli, P.; More, C.; Guigliarelli, B. *J. Am. Chem. Soc.* **1996**, *118*, 1426.
(56) Lill, S.; Siegbahn, P. *Biochemistry* **2009**, *48*, 1056.
(57) Carney, M. J.; Holm, R. H.; Papaefthymiou, G. C.; Frankel, R. B. *J. Am. Chem. Soc.* **1986**, *108*, 3519.
(58) Carney, M. J.; Papaefthymiou, G. C.; Frankel, R. B.; Holm, R. H. *Inorg. Chem.* **1989**, *28*, 1497.
(59) Carney, M. J.; Papaefthymiou, G. C.; Spartalian, K.; Frankel, R. B.; Holm, R. *J. Am. Chem. Soc.* **1988**, *110*, 6084.
(60) Carney, M. J.; Papaefthymiou, G. C.; Whitener, M. A.; Spartalian, K.; Frankel, R. B.; Holm, R. H. *Inorg. Chem.* **1988**, *27*, 346.
(61) Lauterbach, L.; Liu, J.; Horch, M.; Hummel, P.; Schwarze, A.; Haumann, M.; Vincent, K.; Lenz, O.; Zebger, I. *Eur. J. Inorg. Chem.* **2011**, *2011*, 1067.
(62) Kowal, A.; Werth, M.; Manodori, A.; Cecchini, G.; Schroeder, I.; Gunsalus, R.; Johnson, M. *Biochemistry* **1995**, *34*, 12284.
(63) Rothery, R.; Bertero, M.; Cammack, R.; Palak, M.; Blasco, F.; Strynadka, N.; Weiner, J. *Biochemistry* **2004**, *43*, 5324.
(64) George, S. J.; Armstrong, F. A.; Hatchikian, E. C.; Thomson, A. J. *Biochem. J.* **1989**, *264*, 275.
(65) Busch, J. L.; Breton, J. L.; Bartlett, B. M.; Armstrong, F. A.; James, R.; Thomson, A. J. *Biochem. J.* **1997**, *323*, 95.
(66) Duderstadt, R.; Brereton, P.; Adams, M.; Johnson, M. *FEBS Lett.* **1999**, *454*, 21.
(67) Brereton, P.; Duderstadt, R.; Staples, C.; Johnson, M.; Adams, M. *Biochemistry* **1999**, *38*, 10594.
(68) Dementin, S.; Belle, V.; Bertrand, P.; Guigliarelli, B.; Adryanczyk-Perrier, G.; De Lacey, A.; Fernandez, V.; Rousset, M.; Léger, C. *J. Am. Chem. Soc.* **2006**, *128*, 5209.
(69) (a) Teutloff, C.; Löwenstein, J.; Fritsch, J.; Frielingsdorf, S.; Lenz, O.; Lendzian, F.; Bittl, R. In The 45th Annual International Meeting of the EPR Spectroscopy Group of the Royal Society of Chemistry, University of Manchester, U.K., March 25−29, 2012. (b) Frielingsdorf, S.; Fritsch, J.; Hammer, M.; Schmidt, A.; Siebert, E.; Löwenstein, J.; Teutloff, C.; Bittl, R.; Zebger, I.; Hildebrandt, P.; Friedrich, B.; Lenz, O.; Scheerer, P. Unpublished work.
(70) Lees, N. S.; Haenzelmann, P.; Hernandez, H. L.; Subramanian, S.; Schindelin, H.; Johnson, M. K.; Hoffman, B. M. *J. Am. Chem. Soc.* **2009**, *131*, 9184.
(71) Morton, J.; Preston, K. *J. Magn. Reson.* **1978**, *30*, 577.
(72) Mouesca, J. M.; Noodleman, L.; Case, D. A.; Lamotte, B. *Inorg. Chem.* **1995**, *34*, 4347.
(73) Bencini, A.; Gatteschi, D. *EPR of Exchange Coupled Systems*; Springer Verlag: Germany, 1990.
(74) Scholes, C. P.; Lapidot, A.; Mascarenhas, R.; Inubushi, T.; Isaacson, R. A.; Feher, G. *J. Am. Chem. Soc.* **1982**, *104*, 2724.
(75) Zhidomirov, G. M.; Schastnev, P. V.; Chuvylkin, N. D. *Quantum Chemical Calculations of Magnetic Resonance Parameters: Free Radicals*; Novosibirsk: Russia, 1978.
(76) Peters, J. W.; Stowell, M. H. B.; Soltis, S. M.; Finnegan, M. G.; Johnson, M. K.; Rees, D. C. *Biochemistry* **1997**, *36*, 1181.
(77) Grubel, K.; Holland, P. *Angew. Chem., Int. Ed.* **2012**, *51*, 3308.
(78) Horch, M.; Lauterbach, L.; Saggu, M.; Hildebrandt, P.; Lendzian, F.; Bittl, R.; Lenz, O.; Zebger, I. *Angew. Chem., Int. Ed.* **2010**, *49*, 8026.
(79) Trofanchuk, O.; Stein, M.; Geßner, C.; Lendzian, F.; Higuchi, Y.; Lubitz, W. *J. Biol. Inorg. Chem.* **2000**, *5*, 36.